General comments
The manuscript presents a statistical analysis of polarimetric radar data and in-situ (disdrometer)
observations collected over several years in Australia. The topic is relevant for the readership of AMT and the availability of such dataset is very important for future studies. I appreciate that data (and code) are made available. My concerns about this study are related to its objective, in my view not clearly defined, and to the methodological aspects that should be more thoroughly presented. In particular, I expect to see a critical discussion of a few crucial points (comparison of point-measurements with radar volumes, beam broadening effects, gridding of polar data, see the points listed below). I overall recommend a major revision of the manuscript.

We thank the reviewer for their valuable comments. Their suggestions greatly improved the readability of the paper. In particular, the introduction now makes it clearer that the retrieval development and statistical analysis are useful for providing long-term datasets for model validation. In response to other reviewers, we have also revised the PCA section to be easier to interpret by presenting a cross-covariance matrix between the original radar moment and principal component phase space.

We also corrected many typographical and grammar mistakes. We have addressed the reviewer's specific concerns below.

1. The stated objective of this manuscript is to provide (improved) information for validation of global circulation models. However, i do not see any tentative in this direction. The research presented here is a statistical analysis of disdrometer data and radar data in a tropical region. The goal is therefore not clearly defined and it needs some rephrasing / revision.

We have added text in the second and fifth paragraphs of the introduction emphasizing that developing improved rainfall estimates is useful for GCM validation. The goal of the paper is emphasized in the first paragraph of page 4:

"*Creating accurate multidecadal, climate-research quality rainfall rates datasets at TWP Darwin at C- and X-band, as men-tioned previously, is useful for evaluating and improving model predictions. Lately, more radar rainfall estimators at shorter wavelengths have been developed. However, these estimators use data from relatively short field campaigns or a handful of case studies of extreme events. In this regard, these efforts are valuable but potentially not well-matched to the challenges of creating multidecadal datasets at TWP Darwin with a mixture of typical and extreme rainfall events. This therefore stresses the importance of further assessing R retrievals for CPOL and other ARM radars at the ARM TWP site for developing such long-term datasets. To accomplish this task, this study uses four years of co-located two dimensional video disdrometer (VDIS) and CPOL data at the ARM TWP site, providing a longer and therefore hopefully more representative dataset than used in prior Darwin-based studies."*

More detailed specifics of each change are noted in the annotated version of the manuscript with the list of changes made.

2. Should also the distance with respect to the radar be taken into account in your analysis? With in mind attenuation, beam broadening, partial beam filling, it is an important parameter. See also specific comment 3 below.

The CPOL radar has a 1 degree beamwidth.
The range of the gate considered in the comparison from the CPOL radar is 30 km. We now state this in lines 32 to 35 of page 4:
"*At 30 km range, the gate dimensions are 250 m by 260 m, much smaller than a convective cell so the effects of nonuniform beam filling should be minimal. In addition, R estimation errors at C-band due to beam broadening are on the order of 0.2 mm/hr at 30 km range (Gorgucci and Baldini, 2015).***"**

While we acknowledge that analyses of the impact of range on rainfall retrievals are very important, such analyses require a wider rain gauge network than what was available at the ARM TWP site.

We state that we correct for potential (differential) attenuation on lines 9-12 of page 5:
"*The Z-PHI approach provides an estimate of the specific (differential) attenuation (A_{dr}) A_h as a linear function of φ_{dp} that varies depending on the presence of convective "hot spots" (Gu et al., 2011). The A_{dr} and A_h are then integrated along the ray to provide the (differential) attenuation corrected Z_h and Z_{dr}.***"**

3. Section 2.2: i cannot understand a few things in this section. How many disdrometers are used? Where is/are the video-disdrometer(s?) located (a map will help)? . Are they co-located with the radar? Are they distributed in a network? According to which strategy and which assumptions are volume-based radar measurements compared with point-based disdrometer measurements?

Please adapt this section in order to provide the necessary (and very important) information: it is difficult to provide a useful review and relevant suggestions when this aspect is not clear.

We have added a figure showing a map of the location of CPOL and the video and JW disdrometers with discussion in Section 2.

We have also add a sentence in Section 2 denoting our comparison strategy for the rest of the paper:

“*The comparisons in this paper define the point as the average of the data in radial coordinates from the 0.5° PPI scan from the 4 gates closest to the VDIS. This covers a horizontal distance of 0.5-1 km from the VDIS and is about 0.56 km above the VDIS at ground level and 30 km away from CPOL. This definition is chosen as it is consistent with the scales considered in past comparisons by Ryzhkov et al. (2005) and Giangrande et al. (2014a).*”

Specific comments

1. P1: CSU, VDIS: undefined acronyms.

Done as suggested.

2. P2, L1: I would mention also the other fields where accurate rainfall estimation is crucial: nowcasting, alert issuing, climatology (etc.).

We have added these extra uses in page 2, line 1 as suggested.

3. P2, L21: I find this part slightly over-simplified. Beam broadening should be discussed and explained. While the radial resolution can be of 100m in polar coordinates, this will not be true in Cartesian coordinates when we are far from the radar. The conversion from polar data (radar) to Cartesian grid data seems to me a crucial point to discuss, especially given the goal of the manuscript: provide knowledge useful for comparison with global circulation models.

We use do not use the data in Cartesian coordinates, but rather define a point as the average of the 4 gates closest to the VDIS. In Section 2 (line 1-5, p. 5) we now state this:

“*The comparisons in this paper define the point as the average of the data in radial coordinates from the 0.5° PPI scan from the 4 gates closest to the VDIS. This covers a horizontal distance of 0.5-1 km from the VDIS and is about 0.56 km above the VDIS at ground level and 30 km away from CPOL. This definition is chosen as it is consistent with the scales considered in past comparisons by Ryzhkov et al. (2005) and Giangrande et al. (2014a).*”

4. P2, L35: The other side of the medal of ZDR and Kdp is that: (1) they use two channels, so there is twice the possibility that an hardware issue will affect them, (2) Kdp is not a radar observable, but it needs to be estimated from dp: (Otto and Russchenberg, 2011; Wang and Chandrasekar, 2009; Grazioli et al., 2014),

(3) ZDR is affected by differential attenuation and it is affected by the incidence angle (Ryzhkov et al., 2005)

In response to point 1, we have verified that the two channels of CPOL were working correctly for the entire dataset. Since this is implied no text has been added.

In response to point 2, we are aware that Kdp has to be estimated from differential phase and there are sensitivities with errors that are difficult to characterize. However, we do expect that, physically, higher Kdp should indicate the presence of oblate drops which forms the physical basis for dual polarization estimators.

In response to point 3, we apply differential attenuation corrections for ZDR.
In addition, rainfall retrievals typically use a constant elevation (like we do), so incidence angle should not impact the retrieval.

5. P4, L16-20: how are the various elevations combined to provide a proxy of precipitation near ground level?

We use the 0.5 degree PPI scan as a proxy for the precipitation at ground level, as now described in page 5, lines 1-5:

"*The comparisons in this paper define the point as the average of the data in radial coordinates from the 0.5° PPI scan from the 4 gates closest to the VDIS. This covers a horizontal distance of 0.5-1 km from the VDIS and is about 0.56 km above theVDIS at ground level and 30 km away from CPOL. This definition is chosen as it is consistent with the scales considered in past comparisons by Ryzhkov et al. (2005) and Giangrande et al. (2014a).*"

6. Section 4: i had from time to time some difficulties to understand where the polarimetric variables used in this section where coming from (i.e., simulated from VDIS or measured from the radar). I suggest to clarify this aspect through the manuscript, and maybe use a different notation for simulated variables (like ZH).

We have denoted any simulated variables with a ",s" in the subscript for clarity.

7. P12: data availability. Please provide also the link for the data archive.

We have provided the link to ARM Data Discovery (https://www.archive.arm.gov/discovery/).

8. Kdp: a few words about the estimation accuracy of this parameter should be

Kdp processing methods such as LP imply smoothing of the differential phase before the range derivative. Therefore the characterization of the measurement errors of Kdp are not amenable to simple error characterization due to this smoothing.

References

T. Otto and H. W. J. Russchenberg. Estimation of specific differential phase and differential backscatter phase from polarimetric weather radar measurements of rain. IEEE Geosci. Remote Sens. Lett., 8(5):988–992, 2011. doi: 10.1109/LGRS.2011.2145354.

Y. T. Wang and V. Chandrasekar. Algorithm for estimation of the specific differential phase. J. Atmos. Oceanic Technol., 26(12):2565–2578, 2009. doi: 10.1175/2009JTECHA1358.1.

J. Grazioli, M. Schneebeli, and A. Berne. Accuracy of phase-based algorithms for the estimation of the specific differential phase shift using simulated polarimetric weather radar data. IEEE Geosci. Remote Sens. Lett., 11(4):763–767, 2014. doi: 10.1109/LGRS.2013.2278620.

A. V. Ryzhkov, S. E. Giangrande, V. M. Melnikov, and T. J. Schuur. Calibration issues of dual polarization
radar measurements. J. Atmos. Oceanic Technol., 22(8):1138–1155, 2005. doi: 10.1175/JTECH1772.1.

GENERAL COMMENT
This paper presents an analysis of the applicability of dual-polarization rainfall relations for C-band radars. Although in general well written, with adequate reference to previous works and (mostly) clear illustrations, I found the approach presents some flaws, Specifically:

We thank the reviewer for their valuable comments. Their suggestions greatly improved the readability of the paper. In particular we have done the following:

- **Reworked Section 4.2 to both be easier to interpret and to ensure that the dataset is properly normalized and that the correlation between rainfall rate and each principal component is being calculated.**

- **We present the PCA results as a cross-covariance matrix between the original radar observable space and the principal component phase space.**

- **In response to other reviewers we have also reworked the introduction to better emphasize that the retrievals in this study are useful for model-observation intercomparsion.**

- **We also corrected many typographical and grammar mistakes.**

We have addressed the reviewer's specific concerns below and provide an annotated version of the manuscript that shows all of the changes that were made.

- Simulations (section 3.2): the measurement uncertainty is not considered in these simulations. Therefore, these results only show the parametric error. For actual applications, the measurement errors should be included in the simulations. For example, a two-parameter relation like R(Zh,Zdr) has lower parametric error than R(Zh), but may have a larger total error depending on the measurement accuracy of Zdr. Have the actual measurement errors of CPOL been considered somehow?

We thank the reviewer for this insightful comment. We have first added a comment regarding the accuracy of the calibration of Zh and Zdr on lines 8-9, page 5:

"*The RCA technique calibrated Zh to 1 dBZ accuracy and for Zdr to 0.2 dB accuracy (Louf et al., 2019).*"

This level of measurement error particularly affects the utility of Zdr in light rain (page 9, lines 10-12):

"Z_{dr} from CPOL is questionable to use for times when R < 10 mm hr^{-1} as it needs to be accurate within 0.1 dB, less than the quoted 0.2 dB accuracy, for providing reasonable estimates of R in light rain (Ryzhkov et al., 2005)."

But in heavier rainfall (p. 10, line 2):

"*In addition, the 0.2 dB accuracy of Z_{dr} from CPOL is adequate for R estimation in heavier rainfall (Ryzhkov et al., 2005).*"

We also thank the reviewer for providing a more concise name "parametric error" for our results in Section 4.1. We have adopted this terminology throughout the paper.

PCA analysis (section 4.2): this technique is used in this paper as an original contribution for application to dual-polarization radar rainfall estimation. The physical meaning of the results is not always clear. For example, in fig. 5 (panel b) it is not clear if all three lines are the same or something is missing. In panel a) it is a bit confusing to see the first component of Ah close to 0, after having seen an excellent correlation in fig. 3: : : Although I recognize that this can be related to a lack of familiarity with PCA analysis, I encourage to authors to provide more details about the analysis performed and better discussion of the results presented in fig. 5 and 6.

We have reworked this section to ensure that the PCA data are being properly interpreted. In particular, we made the following revisions:

- **Our interpretation of the PCA was only factoring in the variability in the radar observable phase space, but not factoring in how these components also vary with R. We now add the extra step of calculating the correlation of rainfall rate with each principal component.**
- **We standardize our input feature space so that it has zero mean and unit variance to ensure that the differences in units between the variables do not impact the results.**
- **We now show importance matrices, or the absolute value of the cross-covariance matrix between the features in original and PC phase space, in an easier to understand format where higher numbers indicate greater importance of each variable to each principal component.**

I encourage the authors to revise the manuscript, in particular the simulation and PCA analysis sections. Also, the three parts (simulation, PCA analysis, comparison with disdrometer) are treated quite independently and there is little comprehensive discussion in the final section. I would expect in the Conclusions a more in-depth discussion of the key findings and eventually contrasting results obtained with the different methods. As a specific example, I found the conclusion about Ah (it is said that it has little predictive capability) not enough supported by compelling arguments, nor it is considered the fact

that several estimators exist for the estimation of Ah (and for Kdp) with quite different Behavior.

We rewrote the conclusion section to better integrate the results from the three sections by summarizing the consistent conclusions obtained from each of the three steps. Details of these edits are visible in the version of the manuscript with the changes shown.

SPECIFIC COMMENTS AND MINOR CORRECTIONS
- Units should be in Roman font (not Italic), e.g. mm/h.

Done as suggested.

- P2, L4: ": : :magnitude OF the diurnal cycle.."

We have added the "of."

- P3, L25: ".. were developed and using data.." change to ".. were developed using Data.."?

Done as suggested.

- P4, L28-29: "In addition, Zh and Zdr at C-band are prone to (differential) attenuation from heavy rainfall which may bias (underestimate) R". This sentence needs to be reformulated because underestimation of Zdr causes overestimation (not underestimation) of R. In the use of R(Zh,Zdr) estimator, the underestimation of Zh and Zdr due to attenuation tend to (at least partially) compensate because of the opposite sign of the Exponents.

We have changed "underestimate" to now say "overestimate."

- P4, L32: linear programming is used to estimate Kdp. More discussion on this specific estimation method may be needed, especially considering plots like in fig. 8: may the positive biased estimates R(Kdp) at low rain rates may be attributed to the specific behavior of the linear programming algorithm which always produces nonnegative Kdp Values?

Due to factors such as smoothing that is inherent in LP based methods, it is difficult to characterize the potential errors in Kdp produced by such methods.

- P5, L3: "Waldovel" -> "Waldvogel"

Done as suggested.

- P6, L7: “Darwin Colorado”?? Should it read “Darwin (Australia)”?

We added a comma in between Darwin and Colorado.

- P8, L6: normally “PDF” should read better than “p.d.f.”

We now call the “spread in the p.d.f.” parametric error.

- P10, L21: What is the distance between the radar and the VDIS? A map may be useful. It is mentioned that measurements may be affected by attenuation, so it is important to know the range from the radar.

We have added a figure in the paper showing the positions of the radar and the VDIS.

- P12, L6: “based off of limited..” -> “based on”?

Done as suggested.

- P12, L7: “retrieving rainfall retrievals”. May read better: “retrieving rainfall estimates”.

Done as suggested.

- P21, fig.1: panels b) and c) swapped

We have fixed the caption to match the figure.

- P25, fig.5: replace “S-band” with “C-band”?

Done as suggested.

General Comments
This manuscript presents a study of polarimetric relationships to estimate rainfall rates at Darwin, Australia, based on radar retrievals from the C-band dual-polarization radar (CPOL). The retrieved relationships are validated against a co-located two dimensional video disdometer (VDIS) via statistical metrics. I find the manuscript relevant for publication in AMT but I suggest the authors to perform major revisions related mainly to the organization of speech and clarity of explanation throughout the manuscript.

We thank the reviewer for their valuable comments. Their suggestions greatly improved the readability of the paper. In addition to the responses below, other reviewers also asked for more information regarding the experimental setup of the radar and disdrometers, so a figure has been added showing this setup with relevant discussion. A The principal component analysis section has also been rewritten at a reviewer's request in a format that is easier to interpret. Details behind these edits are visible in the attached manuscript with changes noted.

1) For instance, in the Introduction, many of the sentences need a fundamental reorganization (more specifics are presented in the Technical Comments). The overall meaning is understandable but often words are missing or displaced and the flow of the speech is negatively affected.

We have responded to the specific comments regarding the grammar of the paper of the reviewer as below.

2) It is mentioned in the manuscript that the VDIS is co-located with the CPOL radar but no picture of the area where the two sensors are located nor their coordinates are provided by the authors. I suggest to clarify this and include a picture of the filed of study in Darwin.

We have added a figure in Section 2 showing the location of the radar and Disdrometer on a map of the Darwin region.

3) I have some issues with the description of a couple of Figures. In paragraph 3.1 is described Figure 1. A mention is missing of the dashed and solid lines that separate two types of precipitation, even though the selection criteria for convective-stratiform precipitation are described later. Similar remarks apply to Figure 3 and its description in paragraph 3.2. It would be good for a better reader understanding to mention which curve (and in which panel) represents the data fit.

For both of these sections, there is now more text showing the descriptions of these lines in each paragraph.

4) In Section 4.1, it is stated that the Ah-based estimators give the lowest spread for R<10mm/hr and Kdp-based estimators give the lowest spread for R>10mm/hr. This is true only if a combination of different moments is not taken into account but this is not mentioned in the text.

We have rephrased this sentence:
"*In Figures 5ab, the A_h-based estimators give the lowest parametric uncertainty, followed by K_{dp} then Z_h-based estimators for time periods when R < 10 mm hr^{-1} when only a single radar observable is considered.***"**

Specific Comments/Technical Corrections
1) Page 1, line 17. Please define 'VDIS'.

We have changed "VDIS" to say "video disdrometer."

2) Page 2, line 4-5. Please reformulate: 'is that the phase and magnitude the diurnal cycle of precipitation are not adequately resolved due to the parameterization of Convection'.

We have rephrased this sentence to use active voice to make it more readable:

"*A known problem of many GCMs, including the U.S. Department of Energy's Earth Energy Exascale System Model (E3SM), is that GCMs do not adequately resolve the phase and magnitude of the diurnal cycle of precipitation (Golaz et al., 2019). This is due to the fact that GCMs parameterize convection rather than explicitly resolve it (Del Genio, 2012)."*

3) Page 2, line 12-14. Please reformulate the sentence.

This sentence has been simplified:

"In addition to cloud top height and hydrometeor type datasets, long term datasets of accurate rainfall accumulations and rates are also useful for evaluating or improving convective parameterizations in E3SM and other GCMs (Tang et al., 2019)."

4) Page 2, line 15. 'Similar summary'?

Done as suggested.

5) Page 2, line 20. Please replace 'this' with 'a'.

Done as suggested.

6) Page 2, line 22. Please define 'R' in the Introduction.

Done as suggested.

7) Page 3, line 1. Please replace ‘found in the limits of’ with ‘in’.

Done as suggested.

8) Page 3, line 5. Please replace with ‘with DSD observations subject to comparable Limitations’.

Done as suggested.

9) Page 3, line 7. Please insert ‘the’ before ‘aforementioned’.

Done as suggested.

10) Page 3, line 12. Please define ‘DOE ARM’.

Done as suggested..

11) Page 3, line 19. Please define ‘MC3E’.

Done as suggested.

12) Page 3, line 24. Please define ‘RMSE’.

Done as suggested.

13) Page 3, line 25. Please remove ‘and’ before ‘using’.

Done as suggested.

14) Page 3, line 32-33. I don’t understand this sentence. Do you want to state the aim of this research? What are the challenges?

We have revised this line (now lines 5-6, page 4):
“*Creating accurate multidecadal, climate-research quality rainfall rates datasets at TWP Darwin at C- and X-band, as mentioned previously, is useful for evaluating and improving model predictions.***”**

15) Page 3, line 34. ‘Efforts’ don’t have access to data.

We have removed the "efforts" language when this paragraph was reorganized.

16) Page 4, line 7. Please replace 'for' with 'in'.

Done as suggested.

17) Page 4, line 7. No need to say 'rainfall rate R'. Either 'rainfall rate' or 'R' but make sure you defined 'R' previously.

We defined R previously, and removed "rainfall rate."

18) Page 4, line 7. Please use present tense: 'This study uses'.

Done as suggested.

19) Page 4, line 11. 'on these quantities' is superfluous.

Done as suggested.

20) Page 4, line 21. Please remove 'a' before '250 m' and '1'.

Done as suggested.

.

21) Page 4, line 30. Please define 'Z-PHI method' and include a reference.

We have added the description at page 5, lines 8-10:
"The Z-PHI approach provides an estimate of the specific (differential) attenuation (Adr) Ah as a linear function of φdp that varies depending on the presence of convective "hot spots" (Gu et al., 2011)."

22) Page 5, line 4. Are JW disdrometers less optimal for assessing dual-polarization radar efforts in lighter rain and/or small-drop conditions than? And, once again, 'efforts' are not a measurable variable. The authors mean 'radar moments' or 'meteorological Quantities'.

We have rephrased this sentence:
"*However, J-W disdrometers are potentially less optimal for calculating dual-polarization radar quantities in lighter rain and/or small-drop conditions than in heavier rain.***"**

23) Page 5, line 16. Please rephrase as 'After the application of these thresholds'.
C3

Done as suggested.

24) Page 5, line 21. Incorrect reference to Wang et al. (2018) and Giangrande et al. (2019).

Done as suggested.

25) Page 6, line 3. I would not use the verb ‘stratify’ in a sentence where ‘stratiform’ is referred to the type of precipitation. Please use ‘separate’ or ‘divide’.

Done as suggested.

26) Page 6, line 13-14. ‘other datasets around the world’ is too generic.

Done as suggested.

27) Page 6, line 17-18. Please finish the sentence starting with ‘Prior studies find that tropical-oceanic cloud behaviors do not solely drive most of the surface rainfall here’. They drive what else then?

We have rephrased this sentence:

“*Prior studies find that both tropical-oceanic cloud and continental cloud behaviors drive surface rainfall here.***”**

28) Page 6, line 26. Please define ‘W’.

We now define this as liquid water content.

29) Page 6, line 34. The authors mean ‘T15’ here.

Done as suggested.

30) Page 7, line 16. Please add ‘,’ after ‘Therefore’.

Done as suggested.

31) Page 7, line 32-33. The sentence starting with ‘A bootstrap’ is a bit convoluted and needs rephrasing.

We have rephrased this sentence:
Following Wang et al. (2018), Table 2 shows confidence intervals calculated from 1000 fits from 10,000 randomly chosen DSDs, with replacement, from the VDIS dataset.

32) Page 7, line 33 – page 8, line 1. ‘The width of the 95% confidence intervals of a, b, and c of each fit (Table 2) are less than 5% of the mean a, b, and c for each randomly generated fit’. Please mention some numbers in the text for a better understanding.

We have added an approximate order of both the widths of the confidence intervals and the mean of each coefficients to this sentence.

33) Page 8, line 6. Please define ‘p.d.f.’.

This sentence was rephrased to match with newly adopted terminology in the paper.

34) Page 8, line 6,7,9. Be consistent with the use adverbs: ‘firstly’, ‘secondly’, and then ‘Finally’.

Done as suggested.

35) Page 8, line 26. Please remove one instance of ‘only’.

Done as suggested.

36) Page 8, line 29. Please remove ‘use of’.

Done as suggested.

37) Page 9, line 28. Please replace ‘possible’ with ‘possibly’.

Done as suggested.

38) Page 10, line 3. It is valid for X-band radar only based on the figure.

This section was modified in accordance to suggestions of another reviewer with a correct interpretation of the PCA analysis. Therefore, this statement is no longer present.

39) Page 10, line 23. I suggest to mention, for clarity, that the estimator is represented by the dashed line.

Done as suggested.

40) Page 11, line 8. Incorrect reference to ‘Thompson et al. (2018)’
.

We have corrected this citation to use the proper format.

41) Page 11, line 10. Please insert a coma after ‘previous studies’ instead of after

‘Here’.

This comma has been inserted.

42) Page 12, line 4. ‘Algorithms using Ah’ for what?

This has been rephrased to say “R-Ah based estimators” instead of “Algorithms using Ah”

43) Page 12, line 6. Please replace ‘based off of’ with ‘based on’.

This replacement has been done.

44) Page 12, line 7. ‘Therefore’ between comas.

These commas have been inserted.

45) Page 12, line 8. Please use the past tense here: we ‘used’ instead of ‘use’. Check through the manuscript that the tenses are consistent.

The past tense is now used here.

46) Page 12, line 13. ‘The applicability’ to what?

Since the conclusion has been reworked to include more discussion of the three sections, this sentence has been changed to make this comment no longer relevant.

47) Page 12, line 17. Please replace ‘fitted’ with ‘modeled’ or a more exhaustive explanation of the way the fit was performed.

In the reworking of the conclusion, this sentence was removed.

48) Page 12, line 18. Please replace ‘similar’ with ‘similarly’

This sentence has been removed from the manuscript in response to another reviewer.

List of major changes to manuscript

- The PCA analysis has been modified to ensure proper standardization of the data. In addition, the analysis is now presented in terms of cross-covariance matrices between the principal components and also in regards to how each principal component is correlated with rainfall rate. This therefore ensures a more proper interpretation of the PCA results that are easier to understand.
- We have added greater information about the location of the disdrometers and radar to provide greater context to the reader. The location information is vital for understanding how beam broadening and nonuniform beam filling effects can affect the results, so the potential of such effects is also now discussed.
- We include Louf et al. (2019)'s calibration of CPOL as an estimate of the measurement error of reflectivity and differential reflectivity. From this, we interpret the potential applicability of using these two moments in the various rainfall regimes that take this into account.
- We have modified the conclusion to more adequately summarize the results of the paper.
- We have modified the introduction in order to better emphasize the connection between improving rainfall estimates for Darwin and validation of climate models. We emphasize that accurate, long term rainfall observations are useful for climate model validation.
- Grammatical errors noted by the reviewers have been corrected.

References:

Louf, V., A. Protat, R. A. Warren, S. M. Collis, D. B. Wolff, S. Raunyiar, C. Jakob, and W. A. Petersen, An Integrated Approach to Weather Radar Calibration and Monitoring Using Ground Clutter and Satellite Comparisons, *J. Atmos. Oceanic Technol.*, 36, 17–39, https://doi.org/10.1175/JTECH-D-18-0007.1, 2019

*

The development of rainfall retrievals from radar at Darwin

Robert Jackson[1], Scott Collis[1], Valentin Louf[2], Alain Protat[3], Die Wang[4], Scott Giangrande[4], Elizabeth J. Thompson[5], Brenda Dolan[6], and Scott W. Powell[7]

[1]Argonne National Laboratory, 9700 Cass Ave., Lemont, IL, USA
[2]School of Earth, Atmosphere and Environment, Monash University, Clayton, VIC, Australia
[3]Bureau of Meteorology, 700 Clayton St., Docklands, VIC, Australia
[4]Brookhaven National Laboratory, 98 Rochester St., Upton, NY, USA
[5]National Oceanic and Atmospheric Administration Physical Sciences Laboratory, 325 Broadway, Boulder, CO, 80305
[6]Colorado State University, Department of Atmospheric Sciences, 3915 W Laport Ave, Fort Collins, CO 80523
[7]Department of Meteorology, Naval Postgraduate School, Monterey, CA

Correspondence: Robert Jackson (rjackson@anl.gov)

Abstract.

The U.S. Department of Energy Atmospheric Radiation Measurement program Tropical Western Pacific site hosted a C-band POLarization (CPOL) radar in Darwin, Australia. It provides two decades of tropical rainfall characteristics useful for validating global circulation models. Rainfall retrievals from radar assume characteristics about the droplet size distribution (DSD) that vary significantly. To minimize the uncertainty associated with DSD variability, new radar rainfall techniques use dual polarization and specific attenuation estimates. This study challenges the applicability of several specific attenuation and dual-polarization based rainfall estimators in tropical settings using a 4-year archive of Darwin disdrometer datasets in conjunction with CPOL observations. This assessment is based on three metrics: statistical uncertainty estimates, principal component analysis (PCA), and comparisons of various retrievals from CPOL data.

The PCA shows that ~~over 99% of~~ the variability in ~~estimated rainfall rate~~ R can be ~~explained by radar reflectivityfactor for rainfall rates $1 < R < 10$ $mm\ hr^{-1}$~~consistently attributed to reflectivity, but dependence on dual polarization quantities was wavelength dependent for $1 < R < 10$ mm hr^{-1} . These rates primarily originate from stratiform clouds and weak convection (median drop diameters less than 1.5 mm). The dual-polarization specific differential phase ~~increases~~ and differential reflectivity increase in usefulness for rainfall estimators in times with ~~$R > 10$ $mm\ hr^{-1}$~~$R > 10$ mm hr^{-1}. Rainfall estimates during these conditions primarily originate from deep convective clouds with median drop diameters greater than 1.5 mm. ~~Using specific attenuation for estimating R generally does not provide additional skill beyond other metrics for Darwin.~~ An uncertainty analysis and intercomparison with CPOL show that a ~~CSU-blended~~ Colorado State University-blended technique for tropical oceans, with modified estimators developed from ~~VDIS~~ video disdrometer observations, is most appropriate for use in all cases, such as when ~~$1 < R < 10$ $mm\ hr^{-1}$~~ $1 < R < 10$ mm hr^{-1} (stratiform rain), and when ~~$R > 10$ $mm\ hr^{-1}$~~ $R > 10$ mm hr^{-1} (deeper convective rain).

1 Introduction

Accurate rainfall accumulation and rate estimates are crucial for validating global circulation model (GCM) simulations of precipitation and for nowcasting, severe weather alert issuing, and climatology. A known problem of many GCMs, including the U.S. Department of Energy's Earth Energy Exascale System Model (E3SM)~~(Golaz et al., 2019)~~, is that GCMs do not adequately resolve the phase and magnitude of the diurnal cycle of precipitation ~~are not adequately resolved~~ (Golaz et al., 2019) . This is due to the ~~parameterization of convection~~ fact that GCMs parameterize convection rather than explicitly resolve it (Del Genio, 2012). Multidecadal datasets, such as those recorded at the U.S. Department of Energy's Atmospheric Radiation Measurement (ARM) program's Tropical Western Pacific (TWP) site in Darwin, Australia (Keenan et al., 1998; Mather et al., 2016; Long et al., 2016), provide unique opportunities to develop climatologies and process-level parameterization constraints for GCM simulations. For example, Kumar et al. (2013), Rauniyar and Walsh (2016) and Jackson et al. (2018) have previously developed climatologies of radar-estimated cloud top heights from 17 years C-band POLarization (CPOL) data at the ARM TWP site to be used for validation of E3SM. Dolan et al. (2013) also identified the hydrometeor types present in the clouds and precipitation sampled by CPOL over seven seasons.

~~As with the previous~~ In addition to cloud top height and hydrometeor type ~~constraints,~~ datasets, long term datasets of accurate rainfall accumulations and rates are ~~vital quantities to evaluate or improve in models such as in~~ also useful for evaluating or improving convective parameterizations in E3SM ~~(Tang et al., 2019) and other general circulation models for addressing uncertainties in their predictions~~and other GCMs (Tang et al., 2019). The aforementioned CPOL dataset provides 17 wet seasons of precipitation characteristics in Tropical convection, so developing rainfall estimates from ARM radars in TWP aids model validation. However, developing a suitable rainfall rate (R) climatology or similar ~~summary~~ rain accumulation statistics from a single radar dataset is a nontrivial task. Several different methodologies exist for measuring or estimating rainfall accumulations and/or instantaneous rainfall rates. For instance, at the ARM TWP site, rain gauges and disdrometers provide estimates of rainfall rate and collect individual particle statistics. Even if a perfect rainfall estimation method is determined, using such data for climatological scale analysis is complicated by the fact that the rainfall experienced at TWP is not representative of the spatial variability in rainfall rate over GCM-scale domains $O([20-100km])$. In contrast, scanning radars such as the CPOL may estimate rainfall accumulations over ~~this~~ a wider spatial domain $O([100-150km])$ with horizontal resolution of ~~$O(100m)$~~ $O([100m])$ (e.g., Keenan et al. (1998)).

However, scanning radars typically retrieve R using empirical power law relationships between R and the radar observables, which may be subject to uncertainty contingent on the representativeness of these fits. These relations often utilize conventional radar quantities such as the radar reflectivity factor Z_h, and dual-polarization radar quantities such as specific differential phase K_{dp}, and differential reflectivity Z_{dr}. Single-moment and blended empirical relationships are commonplace in the literature (i.e. Marshall and Palmer (1948); Aydin and Giridhar (1992); Ryzhkov and Zrnić (1995); Matrosov (2005); Matrosov et al. (2006); Wang et al. (2013); Ryzhkov et al. (2014); Thompson et al. (2015, 2018); Wang et al. (2018); Giangrande et al.

(2019)) and typically developed from simulated radar moments informed by the drop size distributions (DSDs) sampled by disdrometers at various global locations. Recently, studies have attempted to combine the advantageous dual-polarization radar measurement properties more seamlessly into a single radar quantity by estimating the specific attenuation A_h for similar empirical rainfall applications (e.g., Ryzhkov et al. (2014); Giangrande et al. (2014b)). Dual-polarization relationships have traditionally been the preferable option for radar rainfall rate estimates, as these have been found less sensitive to potential biases owing to DSD variability, radar miscalibration, partial beam blockage, and/or attenuation in rain (Doviak and Zrnić, 1993; Bringi and Chandrasekar, 2001; Ryzhkov et al., 2005). Nevertheless, single and/or dual-polarization power law relationships are often sensitive to the underlying differences ~~found in the limits of the~~ in DSD observations used to develop those relationships, which vary over different regions of the globe due to the changing nature for dominant cloud dynamical/microphysical processes (Bringi et al., 2003, 2009; Dolan et al., 2018). Similar issues are also anticipated for newer radar-rainfall algorithm concepts such as machine learning efforts using Neural Network or Gaussian mixtures concepts (e.g. Vulpiani et al., 2009; Li et al., 2012) that are trained and/or validated ~~within comparable DSD observational~~ with DSD observations subject to comparable limitations.

An important consideration for applying radar rainfall methods to different regions across the globe is that the majority of the aforementioned rainfall studies have emphasized the properties of midlatitude continental clouds, and often over relatively modest data records (i.e. 10s of events). For many practical hydrological applications, the best references are those for NOAA's S-band (10-cm wavelength) NEXt Generation RAdar (NEXRAD), with most operational relations weighted towards Oklahoma, Florida, Colorado and/or deeper convective cloud conditions (Ryzhkov et al., 2005). The relative absence of extended, ground-based rainfall retrieval validation datasets outside of midlatitude regions poses several challenges for potential global rainfall applications and possible model evaluation. ~~DOE ARM~~ The Department of Energy (DOE) Atmospheric Radiation Measurement (ARM) facility operates multiple fixed sites in distinct global regimes, including the Darwin TWP, the Oklahoma Southern Great Plains (SGP) (Sisterson et al., 2016), and Eastern North Atlantic (ENA) site in the Azores (Giangrande et al., 2019). Prior studies that focused on Darwin (Keenan et al., 1998; Bringi et al., 2003, 2009; Thurai et al., 2010) indicate that midlatitude R ~~esimators~~ estimators and DSD variability are less applicable outside of the midlatitudes.

~~This~~ Therefore, as a vital step in providing improved rainfall statistics for model validation, this study focuses on developing R estimators at C-band and X-band ~~for climatological studies and model improvement~~ over Darwin, Australia ~~. Specifically, the ARM TWP site hosts~~ for the purpose of developing long term statistics of rainfall estimates from C/X-band (5 cm/3 cm wavelength) Scanning ARM Precipitation Radars (C/XSAPRs) and ~~the C-band Polarization (CPOL) radar~~ CPOL radar at the ARM TWP site (Keenan et al., 1998). Recently, Giangrande et al. (2014b) found that for the ARM SGP site CSAPR during the ~~MC3E campaign~~Midlatitude Continental Convective Clouds Experiment, K_{dp}-based retrievals generally provide an optimal estimate of rainfall for accumulations greater than 10 mm when compared to A_h-based retrievals. For the tropical oceans, Thompson et al. (2018) showed that the root mean square error (RMSE) between the disdrometer and radar estimated R at C-band and X-band was lowest when the Colorado State University (CSU) blended technique for tropical oceans was used with relations formed from tropical DSD measurements. The algorithm, originally developed by Cifelli et al. (2011), uses Z_h, Z_{dr} and/or K_{dp} as input depending on whether values of these fields are significantly above noise thresholds. In the same

study, RMSE was slightly higher for R estimated by A_h at these wavelengths. However, these retrievals were developed ~~and~~ using data over Manus and Gan Islands. These small atolls experience open-ocean conditions, such that large raindrops from melted hail were rare, even in strong convection (Thompson et al., 2015). For the ARM TWP site in Darwin, deep mixed-phase convection, formed by seabreeze convergence, is common (Rutledge et al., 1992; Williams et al., 1992; May and Rajopadhyaya, 1999; Kumar et al., 2013; May and Ballinger, 2007; Jackson et al., 2018). Therefore, there is greater potential for the impact of cold rain processes (melted hail or graupel that forms large droplets) on determining the surface DSD in Darwin compared to Manus and Gan Islands.

~~It remains unclear whether, or which, prior R estimators are completely suited to the challenges of creating~~ Creating accurate multidecadal, climate-research quality rainfall rates datasets at TWP Darwin at C- and X-band, as mentioned previously, is useful for evaluating and improving model predictions. Lately, more radar rainfall estimators at shorter wavelengths have been developed. However, these ~~efforts typically have access to~~ estimators use data from relatively short field campaigns or a handful of case studies of extreme events. In this regard, these efforts are valuable but potentially not well-matched to the challenges of creating multidecadal datasets at TWP Darwin ~~. This and the lack of studies at sites~~ with a mixture of typical and extreme rainfall events. This therefore stresses the importance of further assessing R retrievals for CPOL and other ARM radars at the ARM TWP site for developing such long-term datasets. To accomplish this task, this study uses four years of co-located two dimensional video disdrometer (VDIS) and CPOL data at the ARM TWP site, providing a longer and therefore hopefully more representative dataset than used in prior Darwin-based studies.

This study is organized as follows. ~~To assess the applicability of dual polarization quantities and an additional estimated quantity A_h for retrieving rainfall rate~~ In order to provide improved R ~~for ARM radars in~~ estimates from ARM radars for Darwin, this study ~~will use~~ uses simulated radar observables and specific attenuation A_h generated from the VDIS observations collected during tropical convective events over the ARM TWP site. Data and methods are introduced in Section 2. Observational results from these data are shown in Section 3. Section 4 assesses the importance of Z_h, Z_{dr}, K_{dp}, and A_h, in determining or informing the rainfall rate estimates over this dataset using principal component analysis (PCA)~~on these quantities~~. These analyses are performed at the C- and X- band radar wavelengths utilized by the ARM program. To evaluate the C-band ~~retrievals~~radar based R estimates, Section 4 also compares VDIS rainfall rates against ~~retrievals~~ R estimates from CPOL data at the ARM Darwin TWP site. Section 5 includes the main conclusions of this study.

2 Datasets

2.1 CPOL

The C-band polarization radar (CPOL) (Keenan et al., 1998) provided plan position indicator (PPI) scans of Z, Z_{dr}, and differential phase ϕ_{dp} at elevations of 0.5°, 0.9°, 1.3°, 1.8°, 2.4°, 3.1°, 4.2°, 5.6°, 7.4°, 10.0°, 13.3°, 17.9°, 23.9°, 32.0°, and 43.1° every 10 minutes from 1998 until 2017 except during 2008 and 2009. Figure 1 shows the location of CPOL and the 2D Video disdrometer (VDIS, also referred to as 2DVD). The maximum unambiguous range of CPOL is 150 km. The Python ARM Radar Toolkit (Py-ART) was used to process and visualize the CPOL data (Helmus and Collis, 2016). Clutter and second

trip echoes were removed using a technique based on the texture of the Doppler velocity field previously applied to CPOL data by Jackson et al. (2018).

Data from the 2011 to 2015 seasons are used in this study, which correspond to the times VDIS observations were available at the ARM TWP site in Darwin 30 km from CPOL. In total, these datasets correspond to a window in time over which the Darwin location recorded 4884 mm of rainfall. CPOL provides radar variables at ~~a~~ 250 m along-gate resolution and ~~a~~ 1° azimuthal resolution. ~~The maximum unambiguous rangeof CPOL is 150 km~~ At 30 km range, the gate dimensions are 250 m by 260 m, much smaller than a convective cell so the effects of nonuniform beam filling should be minimal. In addition, R estimation errors at C-band due to beam broadening are on the order of 0.2 mm/hr at 30 km range (Gorgucci and Baldini, 2015) . The comparisons in this paper define the point as the average of the data in radial coordinates from the 0.5° PPI scan from the 4 gates closest to the VDIS. This covers a horizontal distance of 0.5-1 km from the VDIS and is about 0.56 km above the VDIS at ground level and 30 km away from CPOL. This definition is chosen as it is consistent with the scales considered in past comparisons by Ryzhkov et al. (2005) and Giangrande et al. (2014a). ~~The Python ARM Radar Toolkit (Py-ART) was used to process and visualize the CPOL data (Helmus and Collis, 2016). Clutter and second trip echoes were removed using a technique based on the texture of the Doppler velocity field previously applied to CPOLdata by Jackson et al. (2018).~~

For rainfall retrievals, a robust calibration and attenuation correction of Z_h and Z_{dr} are paramount. Therefore, in this study, Z_h was calibrated using the Relative Calibration Adjustment (RCA) technique (Wolff et al., 2015), previously applied to CPOL data, that integrates the use of ground clutter with space borne radar observations and the self consistency of the polarimetric radar moments to monitor for changes in the radar calibration (as for Darwin CPOL, see Louf et al. (2019)). The RCA technique calibrated Z_h to 1 dBZ accuracy and for Z_{dr} to 0.2 dB accuracy (Louf et al., 2019). In addition, Z_h and Z_{dr} at C-band are prone to (differential) attenuation from heavy rainfall which may bias (~~underestimate~~overestimate) R. ~~Therefore, we apply the~~ The Z-PHI ~~method in order to adjust Z_h and Z_{dr} for attenuation due to heavy rain. This Z-PHI approach also~~ approach provides an estimate of the specific ~~attenuation~~ (differential) attenuation (A_{dr}) A_h as a linear function of ϕ_{dp} that varies depending on the presence of convective "hot spots" (Gu et al., 2011). The A_{dr} and A_h are then integrated along the ray to provide the (differential) attenuation corrected Z_h and Z_{dr}. The ϕ_{dp} was dealiased in order to ensure that it monotonically increases with range. We then applied a linear programming (LP) phase processing technique of Giangrande et al. (2013) to estimate the K_{dp} from these dealiased ϕ_{dp} profiles.

2.2 Disdrometers

Disdrometers are the primary method by which rainfall rates and DSDs parameters are recorded in this study. Previous disdrometer efforts at the ARM TWP Darwin site have explored the extended Darwin ~~Joss-Waldovel~~ Joss-Waldvogel (J-W) disdrometer record (e.g. Giangrande et al., 2014a). However, J-W disdrometers are potentially less optimal for ~~assessing~~ calculating dual-polarization radar ~~efforts~~ quantities in lighter rain and/or small-drop conditions than in heavier rain. Recently, ARM ENA disdrometer comparisons suggested that the ~~2D Video Disdrometer (VDIS , also referred to as 2DVD)~~ VDIS provided improved estimates of the DSD in light rain (Giangrande et al., 2019) compared to the J-W disdrometer. Therefore, we opt to explore the VDIS record to characterize the DSDs and perform subsequent dual-polarization radar quantity calcu-

lations from them. In order to ensure quality DSDs, artifacts that are due to splashing or other causes need to be removed. Following ~~Giangrande et al. (2019) and~~ Wang et al. (2018)'s and Giangrande et al. (2019)'s analysis of VDIS DSDs, thresholds that check drop fall speed and particle diameter were applied to filter out splashing. After ~~that~~the application of these thresholds, the DSDs were averaged to 1 minute to reduce noise and then fitted to a normalized gamma distribution of the form $N(D) = N_w F(D/D_0)$ determined by two parameters N_w and D_0 (Testud et al., 2001). These fits were produced using the method of moments technique in PyDSD (Ulbrich and Atlas, 1998; Hardin and Guy, 2017) utilized in past ARM efforts analyzing VDIS and J-W DSDs (Giangrande et al., 2014a, 2019; Wang et al., 2018). In order to ensure a statistically significant sample required to calculate the gamma distribution parameters, only DSDs with greater than 100 drops and rainfall rates greater than ~~0.5 $mm\ hr^{-1}$~~ $0.5\ \mathrm{mm\ hr^{-1}}$ were included. After these thresholds, 35 211 raining minutes of rain rate and DSD data remained available for use in this study. Changing the drop number threshold to 50, 200, and 500 did not significantly impact the results that follow.

2.3 Radar moment simulations from DSD

For each of the 1-minute DSDs in the VDIS dataset shown in Figure 2, the simulated observables ~~Z_h, Z_{dr}, K_{dp} and A_h~~ $Z_{h,s}$, $Z_{dr,s}$, $K_{dp,s}$ and $A_{h,s}$ were calculated by performing T-matrix scattering simulations (Mishchenko et al., 1996) at C and X-band using Py-TMatrix and PyDSD (Leinonen, 2014; Hardin and Guy, 2017) that has been utilized in past ARM efforts Wang et al. (2018); Giangrande et al. (2019). A drop shape model is required for these simulations. We used Brandes et al. (2002)'s drop size model and a standard deviation of the canting angle of 12°, following Louf et al. (2019)'s CPOL Z_h calibration. The air temperature was assumed to be 20°C for all of the simulations similar to tropical surface air conditions at Darwin. A_h estimates appeared physically consistent with measurements of liquid water content W, which are related to either nearly or exactly the 3rd moment of the DSD, respectively.

3 DSD observations and simulated radar variables from DSD

3.1 DSD parameters

Figure 2 shows N_w, D_0, and R estimated from the VDIS for all DSDs considered. The D_0 distribution is right-tailed, and spans values from 0.5 mm up to 4.5 mm. 90% of the D_0 values are less than 1.8 mm. The N_w spans 5 orders of magnitude and R reached up to ~~150 $mm\ hr^{-1}$~~ $150\ \mathrm{mm\ hr^{-1}}$. Much of this DSD variability is typically attributable to differences in whether the precipitation originates from stratiform or convective clouds and how great of a role is played by ice-based or mixed phase precipitation (i.e. Tokay and Short, 1996; Bringi et al., 2003, 2009; Thompson et al., 2015; Dolan et al., 2018). Therefore, it is important to ~~stratify~~ divide the DSD data by whether they were produced by stratiform and convective clouds. However, different studies have defined stratiform and convective clouds using different thresholds for classification depending on cloud conditions. Bringi et al. (2003), Bringi et al. (2009), and Giangrande et al. (2014a), applied a two-moment DSD-based classification to Darwin datasets such that any DSD having $\log_{10} N_w > 6.3 - 1.6 D_0$ is labelled as convective, whereas

remaining DSDs are marked as stratiform. This relationship, shown by the solid line in Figure 2a, (herein, BR09) was developed using disdrometer data in Darwin, Colorado, and other land locations, enabling deep convective rainfall to be distinguished from widespread stratiform precipitation.

More recently, Thompson et al. (2015) (T15) proposed a definition for Manus and Gan Island that classifies all DSDs with $\log_{10} N_w > 3.8$, as convective, which was consistent with prior work by Bringi et al. (2003, 2009) and Thurai et al. (2010). The T15 relationship is shown as the dashed line in Figure 2a. The T15 definition separated the full range of tropical oceanic convection (weak to strong) from stratiform precipitation. Confirmation for these T15 DSD separations have been subsequently reported by Giangrande et al. (2019) using disdrometers coupled with cloud radar over the ARM oceanic-mid-latitude ENA facility and by Dolan et al. (2018)~~with other datasets around the world~~. Nevertheless, both Thompson et al. (2015)'s oceanic dataset and recent ENA findings do not cover continental-based, deep ice-based convection with hail. Such mixed-phase deep convection and organized convective systems are common over the Darwin region (Williams et al., 1992; Rutledge et al., 1992; May and Rajopadhyaya, 1999; May and Ballinger, 2007; Bringi et al., 2009; Thurai et al., 2010; Jackson et al., 2018). Prior studies find that both tropical-oceanic cloud ~~behaviors do not solely drive most of the~~ and continential cloud behaviors drive surface rainfall here~~, particularly when air flow is from land-to-sea or has significant land-influence~~. These considerations may be analogous to other displays for tropical-continental conditions (Tokay and Short, 1996; Wang et al., 2018), wherein BR09 is typically sufficient to distinguish deeper convective cores from other forms of precipitation. Therefore, this study applies the BR09 convective-stratiform classification to distinguish between the strong convective DSDs and other rain types. We isolate and focus on deep convection in order to study the phenomena most likely to contribute to strong magnitude variability in R. As shown by Thompson et al. (2015) and Dolan et al. (2018), DSDs not classified as convection by BR09 could include contributions from both weak ocean-based convection in addition to stratiform clouds. Here, we simply refer to all non-convective rain classified by BR09 as stratiform.

Figure 3 shows normalized frequency histograms of N_w, D_0, and liquid water content W, separated by the B09 classification. In addition, summary statistics of these variables are given in Table 1. There are 35 211 DSDs in total that fit the filtering criteria used to generate Figure 2. The BR09 classification indicated that 26 131 of these DSDs were not convection. In total, 750 mm, or 21% of the total rainfall accumulation, originated from stratiform rain (Table 1). Past studies in Darwin by Tokay and Short (1996) and Giangrande et al. (2014b) reported that about 30% of the total rainfall accumulation originated from stratiform clouds. Their data and the data here are consistent with the notion that rainfall in Darwin primarily originates from convection. For these stratiform DSDs, W is generally less than ~~1 $g\ m^{-3}$~~ 1 g m^{-3} (Figure 3 and Table 1), from which less attenuation of the radar beam by liquid water is expected and quantified by ~~T18~~T15. The W and D_0 values in Table 1 are lower in stratiform DSDs compared to convective DSDs. The smaller drops in stratiform DSDs for given R shows that these DSDs more likely originated from crystal aggregation aloft in stratiform rain devoid of melting hail (Thurai et al., 2010; Dolan et al., 2018). These relative differences in W, D_0 and N_0 have been shown in Darwin previously (Thurai et al., 2010; Giangrande et al., 2014a).

Convective DSDs exhibited right-tailed distributions of D_0 and left tailed distributions of N_0 and W (Figure 3). In Figure 2, the right tail of D_0 is associated with lower N_0 and W, consistent with fewer and larger drops. This tail has been observed in previous studies in Darwin (Giangrande et al., 2014a) as well as in other regions such as the Amazon (Wang et al., 2018) and

the ARM ENA site (Giangrande et al., 2019). This tail is likely caused by different stages of deep convection being sampled. Large hail grown by accretion that then melts and falls to the ground has very low N_0 and very high D_0 (Bringi et al., 2003, 2009). At the edges of deep convective clouds, size sorting favors fewer, but much larger drops hitting the ground before the more numerous smaller drops do (Gunn and Marshall, 1955; Thompson et al., 2015). In addition, for given ranges of R, there are lower values of N_w and higher values of D_0 in Table 1 for convective DSDs compared to stratiform DSDs. This is consistent with land-based convective-stratiform classification proposed by BR09 using data from Darwin and also other mid-latitude regions such as Colorado.

When looking at histograms of R in Figure 3, it is clear that there is some overlap between convective and stratiform rain DSDs (the stratiform category of BR09 could also include weak oceanic convection, T15). We find that, 95.7% of the DSDs with ~~$R > 10\ mm\ hr^{-1}$~~ $R > 10$ mm hr^{-1} are classified as convective, while 9.7% of the DSDs with ~~$R < 10\ mm\ hr^{-1}$~~ $R < 10$ mm hr^{-1} are convective. This is consistent with prior studies of tropical rain (T15, Rutledge et al., 2019). Therefore, this Darwin data shows that the majority of cases with ~~$R < 10\ mm\ hr^{-1}$~~ $R < 10$ mm hr^{-1} are likely produced by stratiform rain and weak convection while the cases ~~$R > 10\ mm\ hr^{-1}$~~ $R > 10$ mm hr^{-1} are likely the result of deep convection. Therefore, the DSDs collected here are the result of different modes of rain drop formation. Warm rain processes in narrower DSDs are more likely present when ~~$R < 10\ mm\ hr^{-1}$~~ $R < 10$ mm hr^{-1} (T15). Meanwhile, deeper convection where cold rain processes (melting hail) occur is more likely to be present during times when ~~$R > 10\ mm\ hr^{-1}$~~ $R > 10$ mm hr^{-1}. Past studies have used ~~$R = 10\ mm\ hr^{-1}$~~ $R = 10$ mm hr^{-1} as a threshold for separating convective and stratiform DSDs (Tokay and Short, 1996; Nzeukou et al., 2004), so this separation threshold is consistent with past literature examining DSDs in Darwin. However, as shown here and in Giangrande et al. (2014a), thresholds based on R exclude some weak convective events and the lateral edges of strong convection when number concentration is still low.

3.2 Simulated radar moments from DSD

Figure 5 shows scatter plots of R as a function of simulated Z_h, K_{dp}, and A_h at C- and X-band from the VDIS DSDs in Figure 2. The different color lines represent the best fits of R to each of Z_h, K_{dp}, and A_h. In addition, consistent with what has been done in many past studies (i.e. Marshall and Palmer (1948); Aydin and Giridhar (1992); Matrosov (2005); Matrosov et al. (2006); Wang et al. (2013); Ryzhkov et al. (2014); Thompson et al. (2015, 2018); Wang et al. (2018); Giangrande et al. (2019)), Figure 5 and Table 2 show power law fit relationships in the form of $R = aX^b$ or $R = aX^bY^c$. The fits in Table 2 take the linear forms of Z_h, Z_{dr}, and A_h as inputs, denoted as z_h, z_{dr}, and a_h respectively. ~~A bootstrap approach where~~ Following Wang et al. (2018), Table 2 shows confidence intervals calculated from 1000 fits from 10,000 randomly chosen DSDs, with replacement, from the VDIS dataset~~, similar to the approach taken by Wang et al. (2018), provided confidence intervals for each fit~~. The fit ~~curve~~ curves from each of the 1000 fits ~~is~~ are plotted in Figure 5 as black lines. The width of the 95% confidence intervals ($O([10^{-4} - 10^{-3}])$) of a, b, and c of each fit (Table 2) are less than 5% of the mean a, b, and c ($O(1)$) for each randomly generated fit. Furthermore, the randomly generated fits, shown by the black lines in Figure 5, are overlapping in Figure 5, with differences in R less than 10%. This therefore shows that the generated fits are robust.

4 Assessment of applicability of different power law retrievals

Using the 4-year Darwin dataset of DSDs, R, and simulated radar moment data shown in Section 3.2, this section assesses the applicability of dual polarization moments and specific attenuation for R estimation in Darwin. Three criteria will be examined. ~~First~~Firstly, this study estimates the parametric uncertainty in R using the spread in the ~~p.d.f.~~ probability distribution function of R for given ~~radar moments in order to estimate their potential uncertainty incurred in a power-law fit of R from using these moments as input data~~ranges of radar observables. Secondly, ~~a principal component analysis (PCA) is conducted~~ we use principal component to determine whether dual polarization ~~moments~~ quantities or specific attenuation best contribute to the variability in R. This exercise is designed to guide R retrieval development. Finally, the R estimators developed in Section 3.2 are applied to the CPOL dataset and compared against VDIS-observed R in order to test the performance of these retrievals with observed C-band radar data.

4.1 ~~Uncertainty due to use of fit~~Parametric uncertainty

One metric by which the applicability of given radar retrievals can be assessed is by examining the ~~uncertainty, or potential for uncertainty, of the retrieval by considering the spread of~~ parametric uncertainty of R. While in Section 3.2 the bootstrap approach showed that the there is little difference in the power law fits due simply to random sampling, there can be an order of magnitude variability in the distribution of R for a given ~~Z_h, K_{dp}, Z_{dr}, or A_h, creating an uncertainty due to the use of a fit~~$Z_{h,s}$, $K_{dp,s}$, $Z_{dr,s}$, or $A_{h,s}$, showing the potential for large parametric uncertainty. This is why many studies used multiple linear regression, with multiple input variables, to form more constrained power-law R estimators. ~~To define a metric for potential uncertainty in R, this study calculates the spread in the p.d.f~~ This study therefore calculates the parametric uncertainty of R for a given radar observable by subtracting the first quartile of R from the third quartile of R taken over 40 log-uniformly spaced bins of the given radar observable (Kirstetter et al., 2015). The range of these bins are 0 to 70 dBZ for ~~Z_h, $10^{-3} dB\ km^{-1}$ to $100 dB\ km^{-1}$ for A_h, $10^{-3\circ}\ km^{-1}$ to $10^{\circ}\ km^{-1}$ for K_{dp}~~$Z_{h,s}$, 10^{-3} dB km^{-1} to 100 dB km^{-1} for $A_{h,s}$, 10^{-3} $^{\circ}$ km^{-1} to 10 $^{\circ}$ km^{-1} for $K_{dp,s}$, and 0 to 10 dB for ~~Z_{dr}~~$Z_{dr,s}$. The results of these ~~p.d.f spread~~ parametric uncertainty calculations as a function of the mean R over each radar observable bin are shown in Figure 9 for the C- and-X band simulated radar quantities.

In Figures 9ab, the A_h-based estimators give the lowest ~~spreads~~parametric uncertainty, followed by K_{dp}- then Z_h-based estimators for time periods when ~~$R < 10\ mm\ hr^{-1}$~~$R < 10$ mm hr^{-1} when only a single radar observable is considered. However, it is important to note that, at these ~~$R < 10\ mm\ hr^{-1}$~~$R < 10$ mm hr^{-1}, the noisier nature of K_{dp}, and hence A_h makes the applicability of these quantities to R estimators questionable. ~~In fact~~Z_{dr} from CPOL is questionable to use for times when $R < 10$ mm hr^{-1} as it needs to be accurate within 0.1 dB, less than the quoted 0.2 dB accuracy, for providing reasonable estimates of R in light rain (Ryzhkov et al., 2005). In addition, numerous past studies using CSAPR and XSAPR have found the use of K_{dp}- and A_h-based estimators to be only applicable or preferable ~~only~~ for conditions with Z_h > 35-40 dBZ, present at rainfall rates greater than roughly ~~10 $mm\ hr^{-1}$~~10 mm hr^{-1} (Park et al., 2005b, a; Ryzhkov et al., 2005; Giangrande et al., 2014b). Algorithms by Cifelli et al. (2011) and Thompson et al. (2018) use data quality thresholds to avoid ~~use of~~ noisy input data in R estimators. Given that Table 1 shows that the mean ~~Z_h~~ $Z_{h,s}$ is under 40 dBZ for ~~$R < 10\ mm\ hr^{-1}$~~$R < 10$ mm hr^{-1},

this suggests that using the Z_h-based estimators is the most viable option when ~~$1 < R < 10$ mm hr^{-1}~~ $1 < R < 10$ mm hr^{-1}, similar to results using the CSU blended algorithm in Cifelli et al. (2011), Thompson et al. (2018), and Rutledge et al. (2019). However, these Z_h-based estimators produced the highest ~~p.d.f. spreads and greatest R~~ parametric uncertainty, shown in Figure 9 and also quantified by Thompson et al. (2018). The current analysis and these prior studies highlight limitations in estimating light rainfall rates from scanning radars, since they must rely on Z_h in ~~$1 < R < 10$ mm hr^{-1}~~ $1 < R < 10$ mm hr^{-1}.

Looking at ~~$R > 10$ mm hr^{-1}, the p.d.f.s~~ $R > 10$ mm hr^{-1}, the parametric uncertainty of R from K_{dp}-based estimators ~~have the lowest spread~~ are lowest at both C and X band in Figure 9 when only a single radar observable is considered. In the blended algorithm used by Cifelli et al. (2011), Thompson et al. (2018), and Rutledge et al. (2019), K_{dp} is used much more frequently for R estimation at ~~$R >> 10$ mm hr^{-1}~~ $R >> 10$ mm hr^{-1} because it exceeds necessary data quality thresholds. The D_0 was higher in convective DSDs with ~~$R > 10$ mm hr^{-1}~~ $R > 10$ mm hr^{-1} (Table 1), meaning the drop populations were more oblate, produced more total liquid water and rain, and therefore produced significant K_{dp} (Bringi and Chandrasekar, 2001). For instance, in Table 1, D_0 increases from 1.54 mm to 1.77 mm with increasing R when ~~$R > 10$ mm hr^{-1}~~ $R > 10$ mm hr^{-1} for the convective DSDs, also shown by Thompson et al. (2018). By definition, K_{dp} becomes proportional to W and R once drops are large enough to be oblate (Bringi and Chandrasekar, 2001). This is consistent with results that show ~~K_{dp}~~ $K_{dp,s}$ is highly correlated with R when large, oblate drops are present ~~and therefore when $R > 10$ mm hr^{-1}. The spread in R vs K_{dp}~~ when $R > 10$ mm hr^{-1}. The parametric uncertainty in the $R - K_{dp,s}$ relationship is lower for ranges of ~~$R > 10$ mm hr^{-1}~~ $R > 10$ mm hr^{-1} compared to the other observables at the ARM TWP Darwin site when a single radar observable is considered.

Figure 9 shows that the ~~spread in the p.d.f~~ parametric uncertainty is lower when multiple radar observables are considered over the entire range of R compared to when a single observable is used. In particular, the ~~spread in the p.d.f.~~ parametric uncertainty of R is lowest when ~~K_{dp} and Z_{dr}~~ $K_{dp,s}$ and $Z_{dr,s}$ are constrained for time periods when ~~$R > 1.5$ mm hr^{-1}~~ $R > 1.5$ mm hr^{-1}. Even the use of ~~Z_h, and Z_{dr}~~ $Z_{h,s}$, and $Z_{dr,s}$ as constraints lowers the ~~spread in the p.d.f.~~ parametric uncertainty of R compared to using a single radar observable. (K_{dp}, Z_{dr})-based estimators are used to estimate R when ~~$R > 10$ mm hr^{-1}~~ $R > 10$ mm hr^{-1} in the blended algorithm used by Cifelli et al. (2011), Thompson et al. (2018), and Rutledge et al. (2019). In addition, the 0.2 dB accuracy of Z_{dr} from CPOL is adequate for R estimation in heavier rainfall (Ryzhkov et al., 2005). Therefore, similar to past studies in Colorado, Oklahoma, and Manus and Gan Island, this shows that using multiple linear regression reduces the uncertainty in R due to the use of fits for the CPOL data in Darwin.

4.2 Principal component analysis

The previous subsection revealed which rainfall rate estimators most minimize the ~~spread in the p.d.f. of~~ parametric error in R for these Darwin datasets. Now, this section explores the utility of using ~~Z_h, Z_{dr}, K_{dp}, or A_h~~ $Z_{h,s}$, $Z_{dr,s}$, $K_{dp,s}$, or $A_{h,s}$ to estimate R. To do this, ~~this section shows a PCA~~ principal component analysis (PCA) reduces the dimensionality of the feature space by factoring in potential correlations between the variables $Z_{h,s}$, $Z_{dr,s}$, $K_{dp,s}$, and $A_{h,s}$ and creating a new phase space of uncorrelated features. This PCA is conducted on the simulated VDIS radar moments and ~~A_h. The~~ $A_{h,s}$. For PCA, we define a vector $\vec{x} = (Z_{h,s}, A_{h,s}, K_{dp,s}, A_{h,s})$ for each DSD sampled by the VDIS. All such $\vec{x}$ are then the columns of

a matrix $\mathbf{X}$. The first n principal components (PCs) of $\mathbf{X}^T\mathbf{X}$ are then defined to be the first ~~two components explained over 99% of the variance in R. The PCA was applied to A_h, Z_h, and Z_{dr}, in order to minimize variability due to the many orders of magnitude that these variables span. The results of this PCA~~ n normal eigenvectors of $\mathbf{X}^T\mathbf{X}$. The normal eigenvalues λ_n of these eigenvectors show how the variability in the phase space of $\mathbf{X}$ is determined by each PC of $\mathbf{X}$. Since the PCs can be affected by the scale of each row of $\mathbf{X}$, each row of $\mathbf{X}$ is standardized before conducting the PCA. Each column of $\mathbf{X}$ is then projected into a new coordinate system whose basis vectors are each PC and stored into a matrix $\mathbf{X}_p$. From this information, the variable importance matrix $\mathbf{I} = |\mathbf{X}^T\mathbf{X}_p|$, or the absolute value of the cross-covariance matrix between $\mathbf{X}$ and $\mathbf{X}_p$. We then standardize each column of $\mathbf{I}$ to have unit variance so that the values in $\mathbf{I}$ are the absolute values of z-scores. The resulting $\mathbf{I}$ for the simulated radar variables are shown in ~~Figure 10 for C-band and 11for X-band. The explanatory power of the second principal component was small compared to the first, only becoming non-negligible at $R > 100\ mm\ hr^{-1}$ in Figure 10 and at $R > 10\ mm\ hr^{-1}$ Figure 11~~Figures 10 and 11. Three PCs were chosen as over 95% of the variance in $\mathbf{X}$ is explained using three PCs. Finally, in order to determine which PCs contribute to variability in R, we compute the correlation coefficient of the logarithm of R with each row of $\mathbf{X}_p$, as shown in Table 3.

~~The previous analysis in~~ Table 1 and Figure 3 ~~shows~~ show that stratiform and ~~possible~~ possibly weak convective clouds primarily contribute to rainfall for times when ~~$R < 10\ mm\ hr^{-1}$~~ $R < 10$ mm hr^{-1} while stronger convective rain classified by BR98 had higher R. Since we expect rainfall from stratiform and convective clouds to have DSDs with different characteristics for a given R, and ~~$R = 10\ mm\ hr^{-1}$~~ $R = 10$ mm hr^{-1} was a suitable threshold to distinguish deep convection from weaker convection and stratiform rain, the PCA in Figure 10 and 11 ~~is~~ are further stratified by R in order to account for this DSD variability. When restricting the PCA to ~~$1 < R < 10\ mm\ hr^{-1}$, only Z_h explains any of the variance of~~ $1 < R < 10$ mm hr^{-1}, we see that R ~~in Figure 10~~has a stronger correlation (> 0.65) with PC1 than with PC2 and ~~11. This is again~~ PC3 in Table 10b and 11b. $Z_{h,s}$ and $A_{h,s}$ have the greatest contribution to PC1 at C-band, but $Z_{h,s}$ and $Z_{dr,s}$ do at X-band. Therefore, the importance of dual polarization radar quantities and A_h to the variability R for these weaker rainfall conditions is dependent on radar wavelength, but the high importance of Z_h for determining R is consistent across wavelengths. Z_h from CPOL is accurate to within 1 dB Louf et al. (2019), adequate for R estimation in light rain (Ryzhkov et al., 2005), but the calibration of Z_{dr} is not adequate. This is consistent with past efforts that have preferred Z_h estimators for estimating these lighter rainfall rates from scanning radars (Cifelli et al., 2011; Park et al., 2005b; Ryzhkov et al., 2005; Giangrande et al., 2014a, 2019; Thompson et al., 2018; Wang et al., 2018; Rutledge et al., 2019).

~~The second principal component has high absolute values in the K_{dp} and Z_{dr} directions at $10 < R < 100\ mm\ hr^{-1}$. The variance due to the second principal component with higher absolute values in the K_{dp} and Z_{dr} directions starts to exceed 1%, for $R > 100\ mm\ hr^{-1}$. Thus, K_{dp} and Z_{dr} become better suited for~~ For $10 < R < 100$ mm hr^{-1}, the correlation with R ~~estimation as R increases, which confirms prior studies (e. g. Bringi and Chandrasekar (2001)). The first principal component in the K_{dp} direction is 0.25 at $1 < R < 10\ mm\ hr^{-1}$, and~~ with PC1 is still higher (> 0.7~~at $R > 100\ mm\ hr^{-1}$~~) than with PC2 and PC3. However, at $R > 100$ mm hr^{-1}, the correlation of R with PC2 is higher (< -0.6) compared to PC1 and PC3 in Table 3. $Z_{h,s}$ and $Z_{dr,s}$ are the two variables contributing most to the variability in PC1 in Figures 10c and 11c. This relationship is consistent across wavelengths. $K_{dp,s}$ and $Z_{dr,s}$ contribute most to the variability to PC2 in Figures 10cd and 11cd. Therefore,

~~it is clear from this analysis that K_{dp} has more predictive power for~~ as R ~~at these higher rainfall rates~~increases, $K_{dp,s}$ and $Z_{dr,s}$ become better predictors of R. This further confirms and quantifies prior studies that showed K_{dp}-based estimators for R are successful at higher rain rates (Sachidananda and Zrnic', 1985; Sachidananda and Zrnić, 1987). This is also consistent with previous studies recommending the use of K_{dp}-based estimators over A_h-based estimators for CSAPR and XSAPR at the ARM SGP site to sample deep convection (Giangrande et al., 2014b). Finally, this is also consistent with the use of R-(Z_{dr},K_{dp}) estimators in the CSU blended techniques by Cifelli et al. (2011) and Thompson et al. (2015) for these rainfall rates.

~~The PCA shows that A_h has little predictive capability for~~ In this analysis, $A_{h,s}$ is shown to have lower importance to PC1 and PC2 for $R > 10$ mm hr^{-1} in Figures 10bcd and 11bcd compared to $K_{dp,s}$ and $Z_{dr,s}$. While Ryzhkov et al. (2014) demonstrated that, R~~beyond the other observables for DSDs in Darwin except for $R > 100\ mm\ hr^{-1}$ at X-band in Figure 11a.~~ ~~Past~~ A_h are appropriate for use in convection sampled by NEXRAD in Oklahoma, past ARM efforts at SGP have shown that, for XSAPR radars, severe attenuation prohibited accurate rainfall estimation for this range of R (Giangrande et al., 2014b). ~~So, while A_h may provide more predictive capability at X-band at $R > 100\ mm\ hr^{-1}$, it is unlikely that XSAPRs could utilize A_h in these conditions for practice.~~ Therefore, this and the PCA shows that using ~~A_h for developing R estimators for Darwin ARM radars and CPOL, in~~ multiple radar observables in these coastal tropical regions ~~provides no advantage over using other radar observables~~will provide better predictive capability than using A_h alone.

5 Comparisons of CPOL retrievals with VDIS

As a final metric for evaluating the applicability of various radar quantities to the development of R estimators for ARM radars deployed at the TWP ARM site, the R estimators for C-band radars in Section 2.2 were applied to the ~~gate immediately over the VDIS at 0.51 km altitude above ground level~~point above the VDIS as defined in Section 2.1. First, in order to compare the estimators, Figure 12 shows scatter plots of R observed from VDIS compared to observed Z_h, K_{dp} and A_h from CPOL with the R estimator developed from the VDIS data overlaid as a dashed line on the scatter plot. It is apparent that there is one-to-two orders of magnitude of scatter in R, and (~~$RMSE > 8.5\ mm\ hr^{-1}$~~RMSE > 8.5 mm hr^{-1}), in all panels of Figure 12. For Figures 12ac, the Z_h values are generally lower than the fit- produced values for ~~$R > 50\ mm\ hr^{-1}$~~$R > 50$ mm hr^{-1}. While the Z_h are, to the best of possible efforts, adjusted for attenuation, there is still the possibility that Z_h remains affected by attenuation at these high R that was uncorrectable. In addition, factors including the horizontal advection and breakup of drops as they travel from the CPOL sample gate to the VDIS, as well as noise in the K_{dp} and A_h fields at ~~$R < 10\ mm\ hr^{-1}$~~$R < 10$ mm hr^{-1}, are likely inducing scatter. Figure 12 therefore shows that a single radar observable does not adequately describe the full variability of R. As shown in many prior studies, R estimation could be improved by applying a blend of R estimators depending on rain conditions or radar multivariable conditions, or by employing multiple linear regression with more variables in each R estimator.

In order to determine the blend, or set of R estimators based on rain conditions, that can provide the best agreement with VDIS observations, Figure 13 shows comparisons of 10-minute averages of R estimated from CPOL Z_h, A_h, and K_{dp}. The input data to the R estimators are from the CPOL gate immediately over VDIS. The rain-branch of the CSU-blended technique,

originally developed for Colorado by Cifelli et al. (2011), and then subsequently modified for the tropical oceans by Thompson et al. (2018), is also included in Figure 13. The CSU-blended technique uses a decision tree based on data quality thresholds for Z_h, K_{dp}, and Z_{dr} to select an R estimator. The modifications by Thompson et al. (2018) were developed for conditions in Manus and Gan Island where stronger convection that produces hail that can further melt into large surface raindrops is not common. Therefore, since such convection is common in Darwin, the estimators used by the CSU-blended technique to generate Figure 13 were changed to those in Table 2 in order to more accurately represent the local DSDs sampled in Darwin over several years. The data quality thresholds used by ~~(Thompson et al., 2018)~~ Thompson et al. (2018) for tropical oceans were also used here, so only the coefficients of the R estimators were changed.

The analysis, here, and in previous studies, shows that different microphysical processes likely occur at different ranges of R. Namely, raindrops forming from melting hail are unlikely at ~~$1 < R < 10\ mm\ hr^{-1}$~~ $1 < R < 10\ \mathrm{mm\ hr^{-1}}$, but more likely during times when ~~$R > 10\ mm\ hr^{-1}$~~ $R > 10\ \mathrm{mm\ hr^{-1}}$. Therefore, in order to analyze how the agreement between estimated R and VDIS-observed R changes for these different conditions, the mean, 5th, and 95th percentiles of the CPOL estimated R for log-uniformly spaced intervals of VDIS-observed R are shown in Figure 13. The first focus is on time periods with ~~$1 < R < 10\ mm\ hr^{-1}$~~ $1 < R < 10\ \mathrm{mm\ hr^{-1}}$ where stratiform rain and weaker convection are more likely present. ~~It is clear that the mean R estimated by the~~ While the K_{dp}-, (K_{dp},Z_{dr})- and A_h-based estimators ~~greatly overestimate the mean VDIS observed R by over~~ are within a factor of ~~10 for these conditions~~ 2 of VDIS observed R (Figure 13bce), there is greater spread in Figures 13bcd compared to Figures 13aef. However, the mean R from both the CSU-blended technique and the Z_h-based estimators are on average 12% higher than the mean VDIS-observed R (Figure 13af). Consistent with the previous analysis, this again supports the notion that Z_h-based estimators, and the modified CSU-blended technique, are most appropriate for use in these conditions characterized by stratiform and weak convective rainfall.

Switching focus to analyzing conditions of ~~$R > 10\ mm\ hr^{-1}$~~ $R > 10\ \mathrm{mm\ hr^{-1}}$, in which strong convection that is capable of forming hail that melts into raindrops is much more likely, R from CPOL calculated from Z_h- and (Z_h, Z_{dr})-based estimators underestimate the VDIS-observed R (Figure 12ae). On average, the mean estimated R from the modified CSU-blended technique is ~~17~~40% lower than the mean observed R (Figure 13f), while the K_{dp}-estimated R is ~~21% higher~~ 28% lower (Figure 13c), ~~A_r~~ A_h-estimated R is ~~22% higher~~ 52% lower (Figure 13d), and K_{dp}, Z_{dr}-estimated R is ~~36% higher~~ 78% lower (Figure 13d) for these time periods. ~~This~~ However, the spread in Figure 13f is lower than in 13c, showing better correlation between the R estimated from the CSU-blended technique than R from a single estimator. This therefore demonstrates that R estimated from the CSU-blended technique, on average, provides the best agreement with VDIS-observed R for these time periods dominated by stronger convection. The CSU-blended technique also gave estimates of R in best agreement with VDIS-observed R for the time periods dominated by stratiform rain and weaker convection. Therefore, this demonstrates that the use of CSU-blended technique, with modifications to the coefficients of the R estimators for Darwin DSDs, provides the optimal estimate of R for the CPOL data in Darwin.

6 Conclusions

The C-band POLarization (CPOL) Radar at the U.S. Department of Energy Atmospheric Radiation Measurement (ARM) Tropical Western Pacific (TWP) site in Darwin has been operating for over a decade and thus provides an ample dataset for developing essential rainfall climatologies. These ~~are important~~ long term datasets are useful for understanding rainfall variability and for validation of global climate models as well as severe weather forecasts. A crucial quantity in this dataset includes the rainfall rate R. R is not detected directly by radars, but is retrieved from radar observables such as radar reflectivity factor Z_h, differential reflectivity Z_{dr}, specific differential phase K_{dp}, and specific horizontal attenuation A_h. ~~Algorithms using A_h~~ $R - A_h$ estimators at S-band have been successful for the NOAA NEXRAD radars, but studies utilizing ARM C- and X-band scanning radars at the ARM Southern Great Plains site have shown that retrievals using K_{dp} without Z_{dr} are most successful. Most prior studies are based ~~off of~~ on limited data compared to the four year dataset available from ARM TWP Darwin site. This~~therefore~~, therefore, motivated a study to determine which of these radar observables are most applicable for retrieving rainfall ~~retrievals~~ estimates for the CPOL and ARM radars in Darwin. We ~~use~~ used a much larger dataset than previous efforts. We first developed R estimators from simulated ~~Z_h, Z_{dr}, K_{dp}, and A_h~~ $Z_{h,s}$, $Z_{dr,s}$, $K_{dp,s}$, and $A_{h,s}$ from video disdrometer (VDIS) data in Darwin for C- and X-band radar wavelengths. The VDIS observations generally showed that Darwin rainfall is typically stratiform (in terms of frequency), having median drop diameters D_0 less than 1.5 mm at ~~$R < 10\ mm\ hr^{-1}$~~ $R < 10$ mm hr^{-1}. Rainfall here contributed by convection had ~~$D_0 > 1.5\ mm$ for $R > 10\ mm\ hr^{-1}$~~ $D_0 > 1.5$ mm for $R > 10$ mm hr^{-1}, consistent with past observations in Darwin.

~~In order to determine the applicability of Z_h, Z_{dr},~~ Using the simulated data, we examined which radar quantities would likely provide the most utility in developing rainfall estimates from ARM radars in Darwin using a three step approach. First, we assessed the parametric uncertainty of each R estimator produced from the VDIS data. We found that estimators that used multiple observables at once, namely (Z_h, Z_{dr}) and (K_{dp}, Z_{dr}), had the lowest parametric uncertainty. Considering that constraining rainfall rates by parameters that are related to both the shape of the raindrops (K_{dp}, ~~and A_h~~ Z_{dr}) as well as the size and number (Z_h), it is not surprising that the parametric error in R is lower when multiple radar observables are considered. This result is similar to those obtained from previous studies. Therefore, multiple radar observables are required to develop quality rainfall statistics from ARM radars in Darwin.

Secondly, a principal component analysis (PCA) was conducted on ~~Z_h, Z_{dr}, K_{dp}, and A_h simulated~~ $Z_{h,s}$, $Z_{dr,s}$, $K_{dp,s}$, and $A_{h,s}$ from the VDIS DSDs ~~. The majority of the variability in~~ as another metric for determining which quantities had the greatest utility in estimating R~~was attributable to variations in Z_h for $1 < R < 10\ mm\ hr^{-1}$, with K_{dp}~~. While the importance of $Z_{dr,s}$ and $A_{h,s}$ were not consistent across wavelengths when $1 < R < 10$ mm hr^{-1}, $Z_{h,s}$ was a consistent predictor of R for $1 < R < 10$ mm hr^{-1}. Generally, there was a higher number of smaller drops with increasing R in stratiform rain, consistent with crystal aggregation aloft in stratiform rain devoid of melting hail (Thurai et al., 2010; Dolan et al., 2018). $K_{dp,s}$ and $Z_{dr,s}$ becoming increasingly important for explaining R variability at ~~$R > 10\ mm\ hr^{-1}$. A_h provided little additional predictive capability beyond the other observables for R observed by the VDIS for convection over Darwin. The uncertainty in~~ $R > 10$ mm hr^{-1}. Generally, higher median drop sizes were observed in this regime with mostly convective rainfall where

melting hail aloft is more likely to be present (Thurai et al., 2010; Dolan et al., 2018). Therefore, since rain drops become more oblate as they increase in size, the increasing importance of $Z_{dr,s}$ and $K_{dp,s}$ in determining R ~~estimators fitted to these radar inputs was estimated. It was shown that the use of K_{dp}-based estimators, as well as estimators based on multiple observables, minimizes this uncertainty, similar to results from prior studies~~is consistent with the presence of larger drops at higher R. In general, the PCA shows that estimators using multiple radar quantities best characterize the variability observed in R in the simulated VDIS data.

~~To further assess the applicability of the various radar observables to estimating R~~For the third step of this assessment, these different R estimators (formed from simulated VDIS radar variables) were tested on ~~CPOL observations at the radar gate about 0.56 km over the~~ point CPOL observations co-located with the VDIS. Each R estimator was tested individually, and also in the rain-based branch of the CSU Blended algorithm that chooses between estimators based on data quality thresholds (Cifelli et al., 2011; Thompson et al., 2018; Rutledge et al., 2019). ~~The~~ Considering single estimators, R estimated from Z_h was in best agreement with the VDIS when $1 < R < 10$ mm hr^{-1} and R estimated from K_{dp} and Z_{dr} was when $R > 10$ mm hr^{-1}, similar to the choices of estimators used in the CSU-blended algorithm. Not surprisingly, from this, the highest-performing estimation techniques for X- and C- band at Darwin were the CSU-blended technique for rainfall rates of ~~$1 < R < 10\ mm\ hr^{-1}$~~ $1 < R < 10$ mm hr^{-1} as well as when ~~$R > 10\ mm\ hr^{-1}$~~$R > 10$ mm hr^{-1}. This demonstrates that the CSU-blended technique is best for stratiform and weak convective rain as well as strong convection in Darwin. Local R estimators were used in the blended algorithm to more accurately represent DSDs in Darwin. The ~~methodology~~ three steps of this methodology arrive at a consistent conclusion: blended techniques using multiple radar quantities provide the most optimal estimates of R in Darwin due to the wide variability of DSDs observed in Darwin. The methodology used in this study could be used in future studies to quantify uncertainty in R estimation methods.

Code and data availability. The code used for the analysis of the CPOL data is available at http://www.github.com/EVS-ATMOS/cmdv-rrm-anl/. The CPOL data can be downloaded from the Atmospheric Radiation Measurement Facility archive at https://www.archive.arm.gov/discovery/.

Author contributions. RJ conducted most of the data analysis and contributed greatly to the writing of the manuscript. SC, ET, BD, SG, and DW contributed to many of the research ideas and writing in this manuscript. VL and AP processed the CPOL data and provided feedback on the writing of the manuscript. SP provided provided feedback on the writing of the manuscript.

Competing interests. There are no competing interests present in this manuscript.

Acknowledgements. Argonne National Laboratory's work was supported by the U.S. Department of Energy, Office of Science, Office of Biological and Environmental Research, under Contract DE-AC02-06CH11357. This work has been supported by the Office of Biological

and Environmental Research (OBER) of the U.S. Department of Energy (DOE) as part of the Climate Model Development and Validation activity. NOAA PSL contributes effort with funding from the Weather Program Office's Precipitation Prediction Grand Challenge. The development of the Python ARM radar toolkit, was funded by the ARM program part of the Office of Biological and Environmental Research (OBER) of the U.S. Department of Energy (DOE). The work from Monash University and the Bureau of Meteorology was partly supported by the U.S. Department of Energy Atmospheric Systems Research Program through the grant DE-SC0014063. We gratefully acknowledge use of the Bebop cluster in the Laboratory Computing Resource Center at Argonne National Laboratory. The bulk of the code has been written using the open-source NumPy, Scipy, Matplotlib, Jupyter and Dask projects, and the authors are grateful to the authors of these projects. BDs contributions are supported by the U.S. Department of Energy Atmospheric Systems Research Program through the grant DE-SC0017977.

References

Aydin, K. and Giridhar, V.: C-Band Dual-Polarization Radar Observables in Rain, Journal of Atmospheric and Oceanic Technology, 9, 383–390, https://doi.org/10.1175/1520-0426(1992)009<0383:CBDPRO>2.0.CO;2, https://doi.org/10.1175/1520-0426(1992)009<0383:CBDPRO>2.0.CO;2, 1992.

Brandes, E. A., Zhang, G., and Vivekanandan, J.: Experiments in Rainfall Estimation with a Polarimetric Radar in a Subtropical Environment, Journal of Applied Meteorology, 41, 674–685, https://doi.org/10.1175/1520-0450(2002)041<0674:EIREWA>2.0.CO;2, https://doi.org/10.1175/1520-0450(2002)041<0674:EIREWA>2.0.CO;2, 2002.

Bringi, V. N. and Chandrasekar, V.: Radar rainfall estimation, p. 534–569, Cambridge University Press, https://doi.org/10.1017/CBO9780511541094.010, 2001.

Bringi, V. N., Chandrasekar, V., Hubbert, J., Gorgucci, E., Randeu, W. L., and Schoenhuber, M.: Raindrop Size Distribution in Different Climatic Regimes from Disdrometer and Dual-Polarized Radar Analysis, Journal of the Atmospheric Sciences, 60, 354–365, https://doi.org/10.1175/1520-0469(2003)060<0354:RSDIDC>2.0.CO;2, https://doi.org/10.1175/1520-0469(2003)060<0354:RSDIDC>2.0.CO;2, 2003.

Bringi, V. N., Williams, C. R., Thurai, M., and May, P. T.: Using Dual-Polarized Radar and Dual-Frequency Profiler for DSD Characterization: A Case Study from Darwin, Australia, Journal of Atmospheric and Oceanic Technology, 26, 2107–2122, https://doi.org/10.1175/2009JTECHA1258.1, https://doi.org/10.1175/2009JTECHA1258.1, 2009.

Cifelli, R., Chandrasekar, V., Lim, S., Kennedy, P. C., Wang, Y., and Rutledge, S. A.: A New Dual-Polarization Radar Rainfall Algorithm: Application in Colorado Precipitation Events, Journal of Atmospheric and Oceanic Technology, 28, 352–364, https://doi.org/10.1175/2010JTECHA1488.1, https://doi.org/10.1175/2010JTECHA1488.1, 2011.

Del Genio, A. D.: Representing the Sensitivity of Convective Cloud Systems to Tropospheric Humidity in General Circulation Models, Surveys in Geophysics, 33, 637–656, https://doi.org/10.1007/s10712-011-9148-9, https://doi.org/10.1007/s10712-011-9148-9, 2012.

Dolan, B., Rutledge, S. A., Lim, S., Chandrasekar, V., and Thurai, M.: A Robust C-Band Hydrometeor Identification Algorithm and Application to a Long-Term Polarimetric Radar Dataset, Journal of Applied Meteorology and Climatology, 52, 2162–2186, https://doi.org/10.1175/JAMC-D-12-0275.1, https://doi.org/10.1175/JAMC-D-12-0275.1, 2013.

Dolan, B., Fuchs, B., Rutledge, S. A., Barnes, E. A., and Thompson, E. J.: Primary Modes of Global Drop Size Distributions, Journal of the Atmospheric Sciences, 75, 1453–1476, https://doi.org/10.1175/JAS-D-17-0242.1, https://doi.org/10.1175/JAS-D-17-0242.1, 2018.

Doviak, R. J. and Zrnić, D. S.: 8 - Precipitation Measurements, in: Doppler Radar and Weather Observations (Second Edition), edited by Doviak, R. J. and Zrnić, D. S., pp. 209 – 279, Academic Press, San Diego, second edition edn., https://doi.org/https://doi.org/10.1016/B978-0-12-221422-6.50013-9, http://www.sciencedirect.com/science/article/pii/B9780122214226500139, 1993.

Giangrande, S. E., McGraw, R., and Lei, L.: An Application of Linear Programming to Polarimetric Radar Differential Phase Processing, Journal of Atmospheric and Oceanic Technology, 30, 1716–1729, https://doi.org/10.1175/JTECH-D-12-00147.1, https://doi.org/10.1175/JTECH-D-12-00147.1, 2013.

Giangrande, S. E., Bartholomew, M. J., Pope, M., Collis, S., and Jensen, M. P.: A Summary of Precipitation Characteristics from the 2006–11 Northern Australian Wet Seasons as Revealed by ARM Disdrometer Research Facilities (Darwin, Australia), Journal of Applied Meteorology and Climatology, 53, 1213–1231, https://doi.org/10.1175/JAMC-D-13-0222.1, https://doi.org/10.1175/JAMC-D-13-0222.1, 2014a.

Giangrande, S. E., Collis, S., Theisen, A. K., and Tokay, A.: Precipitation Estimation from the ARM Distributed Radar Network during the MC3E Campaign, Journal of Applied Meteorology and Climatology, 53, 2130–2147, https://doi.org/10.1175/JAMC-D-13-0321.1, https://doi.org/10.1175/JAMC-D-13-0321.1, 2014b.

Giangrande, S. E., Wang, D., Bartholomew, M. J., Jensen, M. P., Mechem, D. B., Hardin, J. C., and Wood, R.: Midlatitude Oceanic Cloud and Precipitation Properties as Sampled by the ARM Eastern North Atlantic Observatory, Journal of Geophysical Research: Atmospheres, 124, 4741–4760, https://doi.org/10.1029/2018JD029667, https://agupubs.onlinelibrary.wiley.com/doi/abs/10.1029/2018JD029667, 2019.

Golaz, J.-C., Caldwell, P. M., Van Roekel, L. P., Petersen, M. R., Tang, Q., Wolfe, J. D., Abeshu, G., Anantharaj, V., Asay-Davis, X. S., Bader, D. C., Baldwin, S. A., Bisht, G., Bogenschutz, P. A., Branstetter, M., Brunke, M. A., Brus, S. R., Burrows, S. M., Cameron-Smith, P. J., Donahue, A. S., Deakin, M., Easter, R. C., Evans, K. J., Feng, Y., Flanner, M., Foucar, J. G., Fyke, J. G., Griffin, B. M., Hannay, C., Harrop, B. E., Hunke, E. C., Jacob, R. L., Jacobsen, D. W., Jeffery, N., Jones, P. W., Keen, N. D., Klein, S. A., Larson, V. E., Leung, L. R., Li, H.-Y., Lin, W., Lipscomb, W. H., Ma, P.-L., Mahajan, S., Maltrud, M. E., Mametjanov, A., McClean, J. L., McCoy, R. B., Neale, R. B., Price, S. F., Qian, Y., Rasch, P. J., Reeves Eyre, J. J., Riley, W. J., Ringler, T. D., Roberts, A. F., Roesler, E. L., Salinger, A. G., Shaheen, Z., Shi, X., Singh, B., Tang, J., Taylor, M. A., Thornton, P. E., Turner, A. K., Veneziani, M., Wan, H., Wang, H., Wang, S., Williams, D. N., Wolfram, P. J., Worley, P. H., Xie, S., Yang, Y., Yoon, J.-H., Zelinka, M. D., Zender, C. S., Zeng, X., Zhang, C., Zhang, K., Zhang, Y., Zheng, X., Zhou, T., and Zhu, Q.: The DOE E3SM coupled model version 1: Overview and evaluation at standard resolution, Journal of Advances in Modeling Earth Systems, 0, https://doi.org/10.1029/2018MS001603, https://agupubs.onlinelibrary.wiley.com/doi/abs/10.1029/2018MS001603, 2019.

Gorgucci, E. and Baldini, L.: Influence of Beam Broadening on the Accuracy of Radar Polarimetric Rainfall Estimation, Journal of Hydrometeorology, 16, 1356–1371, https://doi.org/10.1175/JHM-D-14-0084.1, https://doi.org/10.1175/JHM-D-14-0084.1, 2015.

Gu, J.-Y., Ryzhkov, A., Zhang, P., Neilley, P., Knight, M., Wolf, B., and Lee, D.-I.: Polarimetric Attenuation Correction in Heavy Rain at C Band, Journal of Applied Meteorology and Climatology, 50, 39–58, https://doi.org/10.1175/2010JAMC2258.1, https://doi.org/10.1175/2010JAMC2258.1, 2011.

Gunn, K. L. S. and Marshall, J. S.: THE EFFECT OF WIND SHEAR ON FALLING PRECIPITATION, Journal of Meteorology, 12, 339–349, https://doi.org/10.1175/1520-0469(1955)012<0339:TEOWSO>2.0.CO;2, https://doi.org/10.1175/1520-0469(1955)012<0339:TEOWSO>2.0.CO;2, 1955.

Hardin, J. and Guy, N.: PyDisdrometer v1.0, https://doi.org/10.5281/zenodo.9991, https://doi.org/10.5281/zenodo.9991, 2017.

Helmus, J. and Collis, S.: The Python ARM Radar Toolkit (Py-ART), a Library for Working with Weather Radar Data in the Python Programming Language, Journal of Open Research Software, 4, https://doi.org/10.5334/jors.119, http://openresearchsoftware.metajnl.com/articles/10.5334/jors.119/, 2016.

Jackson, R. C., Collis, S. M., Louf, V., Protat, A., and Majewski, L.: A 17 year climatology of convective cloud top heights in Darwin, Atmospheric Chemistry and Physics Discussions, 2018, 1–26, https://doi.org/10.5194/acp-2018-408, https://www.atmos-chem-phys-discuss.net/acp-2018-408/, 2018.

Keenan, T., Glasson, K., Cummings, F., Bird, T. S., Keeler, J., and Lutz, J.: The BMRC/NCAR C-Band Polarimetric (C-POL) Radar System, Journal of Atmospheric and Oceanic Technology, 15, 871–886, https://doi.org/10.1175/1520-0426(1998)015<0871:TBNCBP>2.0.CO;2, https://doi.org/10.1175/1520-0426(1998)015<0871:TBNCBP>2.0.CO;2, 1998.

Kirstetter, P.-E., Gourley, J. J., Hong, Y., Zhang, J., Moazamigoodarzi, S., Langston, C., and Arthur, A.: Probabilistic precipitation rate estimates with ground-based radar networks, Water Resources Research, 51, 1422–1442, https://doi.org/10.1002/2014WR015672, https://agupubs.onlinelibrary.wiley.com/doi/abs/10.1002/2014WR015672, 2015.

Kumar, V. V., Protat, A., May, P. T., Jakob, C., Penide, G., Kumar, S., and Davies, L.: On the Effects of Large-Scale Environment and Surface Types on Convective Cloud Characteristics over Darwin, Australia, Monthly Weather Review, 141, 1358–1374, https://doi.org/10.1175/MWR-D-12-00160.1, https://doi.org/10.1175/MWR-D-12-00160.1, 2013.

Leinonen, J.: High-level interface to T-matrix scattering calculations: architecture, capabilities and limitations, Opt. Express, 22, 1655–1660, https://doi.org/10.1364/OE.22.001655, http://www.opticsexpress.org/abstract.cfm?URI=oe-22-2-1655, 2014.

Li, Z., Zhang, Y., and Giangrande, S. E.: Rainfall-Rate Estimation Using Gaussian Mixture Parameter Estimator: Training and Validation, Journal of Atmospheric and Oceanic Technology, 29, 731–744, https://doi.org/10.1175/JTECH-D-11-00122.1, https://doi.org/10.1175/JTECH-D-11-00122.1, 2012.

Long, C. N., Mather, J. H., and Ackerman, T. P.: The ARM Tropical Western Pacific (TWP) Sites, Meteorological Monographs, 57, 7.1–7.14, https://doi.org/10.1175/AMSMONOGRAPHS-D-15-0024.1, https://doi.org/10.1175/AMSMONOGRAPHS-D-15-0024.1, 2016.

Louf, V., Protat, A., Warren, R. A., Collis, S. M., Wolff, D. B., Raunyiar, S., Jakob, C., and Petersen, W. A.: An Integrated Approach to Weather Radar Calibration and Monitoring Using Ground Clutter and Satellite Comparisons, Journal of Atmospheric and Oceanic Technology, 36, 17–39, https://doi.org/10.1175/JTECH-D-18-0007.1, https://doi.org/10.1175/JTECH-D-18-0007.1, 2019.

Marshall, J. S. and Palmer, W. M. K.: THE DISTRIBUTION OF RAINDROPS WITH SIZE, Journal of Meteorology, 5, 165–166, https://doi.org/10.1175/1520-0469(1948)005<0165:TDORWS>2.0.CO;2, https://doi.org/10.1175/1520-0469(1948)005<0165:TDORWS>2.0.CO;2, 1948.

Mather, J. H., Turner, D. D., and Ackerman, T. P.: Scientific Maturation of the ARM Program, Meteorological Monographs, 57, 4.1–4.19, https://doi.org/10.1175/AMSMONOGRAPHS-D-15-0053.1, https://doi.org/10.1175/AMSMONOGRAPHS-D-15-0053.1, 2016.

Matrosov, S. Y.: Attenuation-Based Estimates of Rainfall Rates Aloft with Vertically Pointing Ka-Band Radars, Journal of Atmospheric and Oceanic Technology, 22, 43–54, https://doi.org/10.1175/JTECH-1677.1, https://doi.org/10.1175/JTECH-1677.1, 2005.

Matrosov, S. Y., Cifelli, R., Kennedy, P. C., Nesbitt, S. W., Rutledge, S. A., Bringi, V. N., and Martner, B. E.: A Comparative Study of Rainfall Retrievals Based on Specific Differential Phase Shifts at X- and S-Band Radar Frequencies, Journal of Atmospheric and Oceanic Technology, 23, 952–963, https://doi.org/10.1175/JTECH1887.1, https://doi.org/10.1175/JTECH1887.1, 2006.

May, P. T. and Ballinger, A.: The Statistical Characteristics of Convective Cells in a Monsoon Regime (Darwin, Northern Australia), Monthly Weather Review, 135, 82–92, https://doi.org/10.1175/MWR3273.1, https://doi.org/10.1175/MWR3273.1, 2007.

May, P. T. and Rajopadhyaya, D. K.: Vertical Velocity Characteristics of Deep Convection over Darwin, Australia, Monthly Weather Review, 127, 1056–1071, https://doi.org/10.1175/1520-0493(1999)127<1056:VVCODC>2.0.CO;2, https://doi.org/10.1175/1520-0493(1999)127<1056:VVCODC>2.0.CO;2, 1999.

Mishchenko, M. I., Travis, L. D., and Mackowski, D. W.: T-matrix computations of light scattering by nonspherical particles: A review, Journal of Quantitative Spectroscopy and Radiative Transfer, 55, 535 – 575, https://doi.org/https://doi.org/10.1016/0022-4073(96)00002-7, http://www.sciencedirect.com/science/article/pii/0022407396000027, light Scattering by Non-Spherical Particles, 1996.

Nzeukou, A., Sauvageot, H., Ochou, A. D., and Kebe, C. M. F.: Raindrop Size Distribution and Radar Parameters at Cape Verde, Journal of Applied Meteorology, 43, 90–105, https://doi.org/10.1175/1520-0450(2004)043<0090:RSDARP>2.0.CO;2, https://doi.org/10.1175/1520-0450(2004)043<0090:RSDARP>2.0.CO;2, 2004.

Park, S.-G., Bringi, V. N., Chandrasekar, V., Maki, M., and Iwanami, K.: Correction of Radar Reflectivity and Differential Reflectivity for Rain Attenuation at X Band. Part I: Theoretical and Empirical Basis, Journal of Atmospheric and Oceanic Technology, 22, 1621–1632, https://doi.org/10.1175/JTECH1803.1, https://doi.org/10.1175/JTECH1803.1, 2005a.

Park, S.-G., Maki, M., Iwanami, K., Bringi, V. N., and Chandrasekar, V.: Correction of Radar Reflectivity and Differential Reflectivity for Rain Attenuation at X Band. Part II: Evaluation and Application, Journal of Atmospheric and Oceanic Technology, 22, 1633–1655, https://doi.org/10.1175/JTECH1804.1, https://doi.org/10.1175/JTECH1804.1, 2005b.

Rauniyar, S. and Walsh, K.: Spatial and temporal variations in rainfall over Darwin and its vicinity during different large-scale environments, Climate Dynamics, 46, https://doi.org/10.1007/s00382-015-2606-1, https://doi.org/10.1007/s00382-015-2606-1, 2016.

Rutledge, S. A., Williams, E. R., and Keenan, T. D.: The Down Under Doppler and Electricity Experiment (DUNDEE): Overview and Preliminary Results, Bulletin of the American Meteorological Society, 73, 3–16, https://doi.org/10.1175/1520-0477(1992)073<0003:TDUDAE>2.0.CO;2, https://doi.org/10.1175/1520-0477(1992)073<0003:TDUDAE>2.0.CO;2, 1992.

Rutledge, S. A., Chandrasekar, V., Fuchs, B., George, J., Junyent, F., Dolan, B., Kennedy, P. C., and Drushka, K.: SEA-POL Goes to Sea, Bulletin of the American Meteorological Society, 100, 2285–2301, https://doi.org/10.1175/BAMS-D-18-0233.1, https://doi.org/10.1175/BAMS-D-18-0233.1, 2019.

Ryzhkov, A., Diederich, M., Zhang, P., and Simmer, C.: Potential Utilization of Specific Attenuation for Rainfall Estimation, Mitigation of Partial Beam Blockage, and Radar Networking, Journal of Atmospheric and Oceanic Technology, 31, 599–619, https://doi.org/10.1175/JTECH-D-13-00038.1, https://doi.org/10.1175/JTECH-D-13-00038.1, 2014.

Ryzhkov, A. V. and Zrnić, D. S.: Comparison of Dual-Polarization Radar Estimators of Rain, Journal of Atmospheric and Oceanic Technology, 12, 249–256, https://doi.org/10.1175/1520-0426(1995)012<0249:CODPRE>2.0.CO;2, https://doi.org/10.1175/1520-0426(1995)012<0249:CODPRE>2.0.CO;2, 1995.

Ryzhkov, A. V., Giangrande, S. E., Melnikov, V. M., and Schuur, T. J.: Calibration Issues of Dual-Polarization Radar Measurements, Journal of Atmospheric and Oceanic Technology, 22, 1138–1155, https://doi.org/10.1175/JTECH1772.1, https://doi.org/10.1175/JTECH1772.1, 2005.

Sachidananda, M. and Zrnic', D. S.: ZDR measurement considerations for a fast scan capability radar, Radio Science, 20, 907–922, https://doi.org/10.1029/RS020i004p00907, https://agupubs.onlinelibrary.wiley.com/doi/abs/10.1029/RS020i004p00907, 1985.

Sachidananda, M. and Zrnić, D. S.: Rain Rate Estimates from Differential Polarization Measurements, Journal of Atmospheric and Oceanic Technology, 4, 588–598, https://doi.org/10.1175/1520-0426(1987)004<0588:RREFDP>2.0.CO;2, https://doi.org/10.1175/1520-0426(1987)004<0588:RREFDP>2.0.CO;2, 1987.

Sisterson, D. L., Peppler, R. A., Cress, T. S., Lamb, P. J., and Turner, D. D.: The ARM Southern Great Plains (SGP) Site, Meteorological Monographs, 57, 6.1–6.14, https://doi.org/10.1175/AMSMONOGRAPHS-D-16-0004.1, https://doi.org/10.1175/AMSMONOGRAPHS-D-16-0004.1, 2016.

Tang, Q., Klein, S. A., Xie, S., Lin, W., Golaz, J.-C., Roesler, E. L., Taylor, M. A., Rasch, P. J., Bader, D. C., Berg, L. K., Caldwell, P., Giangrande, S. E., Neale, R. B., Qian, Y., Riihimaki, L. D., Zender, C. S., Zhang, Y., and Zheng, X.: Regionally refined test bed in E3SM atmosphere model version 1 (EAMv1) and applications for high-resolution modeling, Geoscientific Model Development, 12, 2679–2706, https://doi.org/10.5194/gmd-12-2679-2019, https://www.geosci-model-dev.net/12/2679/2019/, 2019.

Testud, J., Oury, S., Black, R. A., Amayenc, P., and Dou, X.: The Concept of "Normalized" Distribution to Describe Raindrop Spectra: A Tool for Cloud Physics and Cloud Remote Sensing, Journal of Applied Meteorology, 40, 1118–1140, https://doi.org/10.1175/1520-0450(2001)040<1118:TCONDT>2.0.CO;2, https://doi.org/10.1175/1520-0450(2001)040<1118:TCONDT>2.0.CO;2, 2001.

Thompson, E. J., Rutledge, S. A., Dolan, B., and Thurai, M.: Drop Size Distributions and Radar Observations of Convective and Stratiform Rain over the Equatorial Indian and West Pacific Oceans, Journal of the Atmospheric Sciences, 72, 4091–4125, https://doi.org/10.1175/JAS-D-14-0206.1, https://doi.org/10.1175/JAS-D-14-0206.1, 2015.

Thompson, E. J., Rutledge, S. A., Dolan, B., Thurai, M., and Chandrasekar, V.: Dual-Polarization Radar Rainfall Estimation over Tropical Oceans, Journal of Applied Meteorology and Climatology, 57, 755–775, https://doi.org/10.1175/JAMC-D-17-0160.1, https://doi.org/10.1175/JAMC-D-17-0160.1, 2018.

Thurai, M., Bringi, V. N., and May, P. T.: CPOL Radar-Derived Drop Size Distribution Statistics of Stratiform and Convective Rain for Two Regimes in Darwin, Australia, Journal of Atmospheric and Oceanic Technology, 27, 932–942, https://doi.org/10.1175/2010JTECHA1349.1, https://doi.org/10.1175/2010JTECHA1349.1, 2010.

Tokay, A. and Short, D. A.: Evidence from Tropical Raindrop Spectra of the Origin of Rain from Stratiform versus Convective Clouds, Journal of Applied Meteorology, 35, 355–371, https://doi.org/10.1175/1520-0450(1996)035<0355:EFTRSO>2.0.CO;2, https://doi.org/10.1175/1520-0450(1996)035<0355:EFTRSO>2.0.CO;2, 1996.

Ulbrich, C. W. and Atlas, D.: Rainfall Microphysics and Radar Properties: Analysis Methods for Drop Size Spectra, Journal of Applied Meteorology, 37, 912–923, https://doi.org/10.1175/1520-0450(1998)037<0912:RMARPA>2.0.CO;2, https://doi.org/10.1175/1520-0450(1998)037<0912:RMARPA>2.0.CO;2, 1998.

Vulpiani, G., Giangrande, S., and Marzano, F. S.: Rainfall Estimation from Polarimetric S-Band Radar Measurements: Validation of a Neural Network Approach, Journal of Applied Meteorology and Climatology, 48, 2022–2036, https://doi.org/10.1175/2009JAMC2172.1, https://doi.org/10.1175/2009JAMC2172.1, 2009.

Wang, D., Giangrande, S. E., Bartholomew, M. J., Hardin, J., Feng, Z., Thalman, R., and Machado, L. A. T.: The Green Ocean: precipitation insights from the GoAmazon2014/5 experiment, Atmospheric Chemistry and Physics, 18, 9121–9145, https://doi.org/10.5194/acp-18-9121-2018, https://www.atmos-chem-phys.net/18/9121/2018/, 2018.

Wang, H., Easter, R. C., Rasch, P. J., Wang, M., Liu, X., Ghan, S. J., Qian, Y., Yoon, J.-H., Ma, P.-L., and Vinoj, V.: Sensitivity of remote aerosol distributions to representation of cloud–aerosol interactions in a global climate model, Geoscientific Model Development, 6, 765–782, https://doi.org/10.5194/gmd-6-765-2013, https://www.geosci-model-dev.net/6/765/2013/, 2013.

Williams, E. R., Geotis, S. G., Renno, N., Rutledge, S. A., Rasmussen, E., and Rickenbach, T.: A Radar and Electrical Study of Tropical "Hot Towers", Journal of the Atmospheric Sciences, 49, 1386–1395, https://doi.org/10.1175/1520-0469(1992)049<1386:ARAESO>2.0.CO;2, https://doi.org/10.1175/1520-0469(1992)049<1386:ARAESO>2.0.CO;2, 1992.

Wolff, D. B., Marks, D. A., and Petersen, W. A.: General Application of the Relative Calibration Adjustment (RCA) Technique for Monitoring and Correcting Radar Reflectivity Calibration, Journal of Atmospheric and Oceanic Technology, 32, 496–506, https://doi.org/10.1175/JTECH-D-13-00185.1, https://doi.org/10.1175/JTECH-D-13-00185.1, 2015.

Table 1. Mean DSD parameters for given R ranges and BR09 convective-stratiform classification.

R range [$\mathrm{mm\ hr^{-1}}$]	No DSD		Mean R [$\mathrm{mm\ hr^{-1}}$]		$\log_{10} N_w$ [$\mathrm{m^{-3}\ mm^{-1}}$]		D_0 [mm]		Z_h [dBZ]		W [$\mathrm{g\ m^{-3}}$]	
	C	S	C	S	C	S	C	S	C	S	C	S
0.5-2	679	15052	1.06	1.07	2.40	1.17	2.29	3.38	4.0	24.8	0.06	0.05
2-4	443	6568	2.97	2.85	3.08	3.66	1.96	1.26	32.1	30.5	0.14	0.13
4-6	436	2694	5.00	4.84	3.38	3.89	1.79	1.27	34.8	33.2	0.24	0.23
6-10	1216	1536	8.08	7.36	3.85	4.13	1.54	1.23	36.3	35.2	0.39	0.36
10-20	2422	257	14.3	12.6	4.07	4.34	1.52	1.24	39.5	39.7	0.69	0.60
20-40	2036	24	28.5	25.4	4.19	4.53	1.66	1.32	44.2	48.3	1.33	1.24
40-60	956	0	48.9	n/a	4.32	n/a	1.75	n/a	48.1	n/a	2.30	n/a
60+	887	0	85.9	n/a	4.54	n/a	1.77	n/a	51.5	n/a	4.11	n/a

Table 2. 95% confidence intervals of the generated fit parameters, RMSE, and correlation coefficient for each fit.

Relationship	**a**	**b**	**c**	**RMSE** [$\mathrm{mm\ hr^{-1}}$]	**Correlation Coefficient**
C-band					
$R(z_h)$	0.0208 ± 0.00	$0.66\ \pm 0.0002$		16.66	0.95
$R(z_h)$ convective	0.0607 $\pm$0.00002	0.60 $\pm$0.0001		35.30	0.91
$R(z_h)$ stratiform	0.0438 $\pm$0.00005	0.56 $\pm$0.0002		2.75	0.90
$R(K_{dp})$	26.116 ± 0.01	0.77 ± 0.0001		4.67	0.96
$R(a_h)$	258.89 ± 0.31	0.87 ± 0.0002		12.76	0.79
$R(\mathrm{z}_h, \mathrm{z}_{dr})$	0.0122 ± 0.0000	0.85 ± 0.0002	-4.25 ± 0.006	4.09	0.97
$R(K_{dp}, z_{dr})$	46.2347 ± 0.06	0.90 ± 0.0002	$-1.69\ \pm 0.006$	3.86	0.99
X-band					
$R(z_h)$	0.0369 $\pm$0.00004	0.61 $\pm$0.000		16.03	0.94
$R(z_h)$ convective	0.1056 $\pm$0.00003	0.53 $\pm$0.000		35.2	0.88
$R(z_h)$ stratiform	0.0369 $\pm$0.00006	0.67 $\pm$0.000		2.79	0.89
$R(K_{dp})$	17.5432 $\pm$0.006	0.77 $\pm$0.0001		4.38	0.97
$R(a_h)$	49.54 $\pm$0.027	0.80 $\pm$0.0001		5.56	0.79
$R(z_h, z_{dr})$	0.011 $\pm$0.00001	0.89 $\pm$0.0001	-5.35 $\pm$0.002	4.20	0.98
$R(K_{dp}, z_{dr})$	31.794 $\pm$0.017	0.94 $\pm$0.0001	-1.99 $\pm$0.002	3.88	0.98

Table 3. Correlation coefficients between R and each PC.

C-band	**PC1**	**PC2**	**PC3**
all data	0.84	-0.48	0.12
1 to 10 mm hr^{-1}	0.66	-0.42	0.54
10 to 100 mm hr^{-1}	0.73	-0.62	0.18
100+ mm hr^{-1}	0.53	-0.67	0.39
X-band			
all data	0.86	0.33	-0.35
1 to 10 mm hr^{-1}	0.69	-0.64	-0.13
10 to 100 mm hr^{-1}	0.80	-0.54	-0.20
100+ mm hr^{-1}	0.52	-0.76	0.00

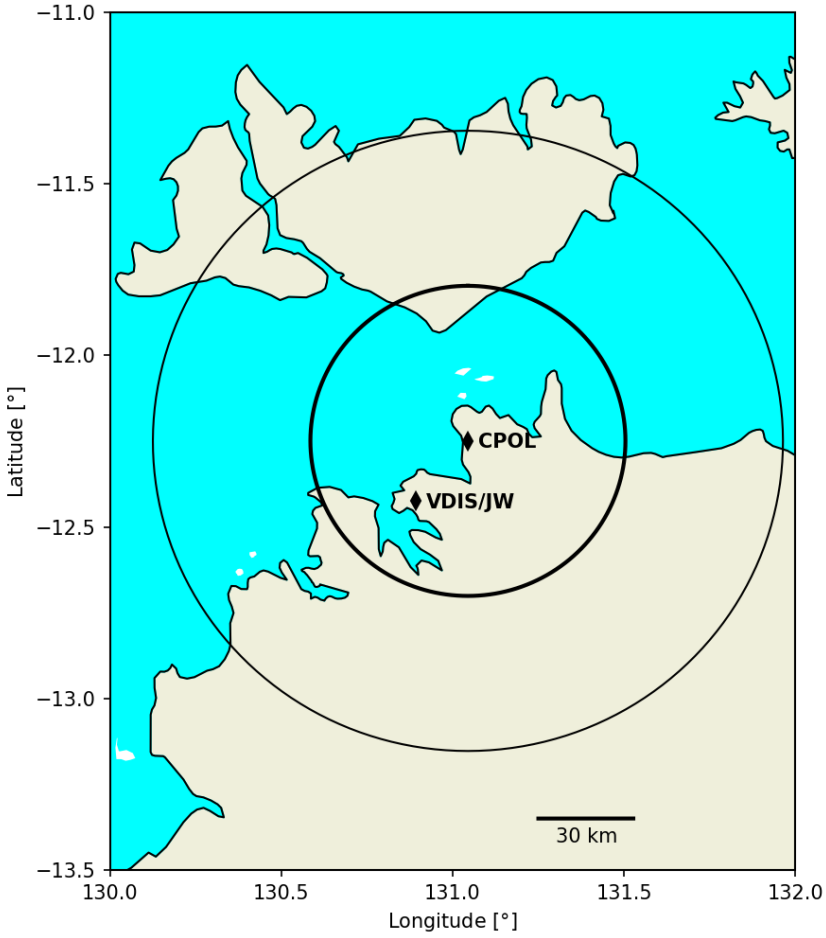

Figure 1. Map of CPOL and JW/VDIS locations. Range rings represent distances 50 and 100 km from the radar.

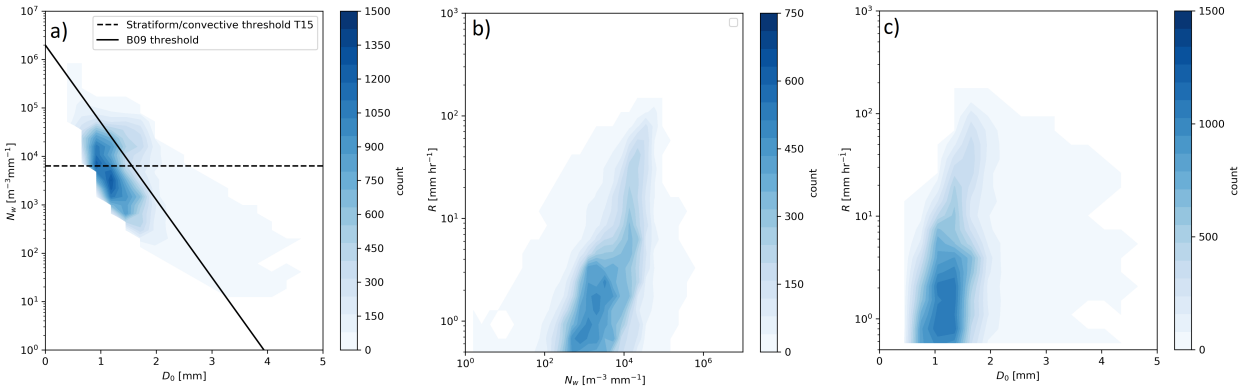

Figure 2. Frequency histogram of **(a)** N_w and D_0, **(b)** R and ~~D~~N~~0~~w, and **(c)** R and ~~N~~D~~w~~0from the VDIS for all of the DSDs containing more than 100 drops in each sample. The criteria used to classify stratiform and convective DSDs from Bringi et al. (2009) (BR09) and Thompson et al. (2015) (T15) are shown by the lines.

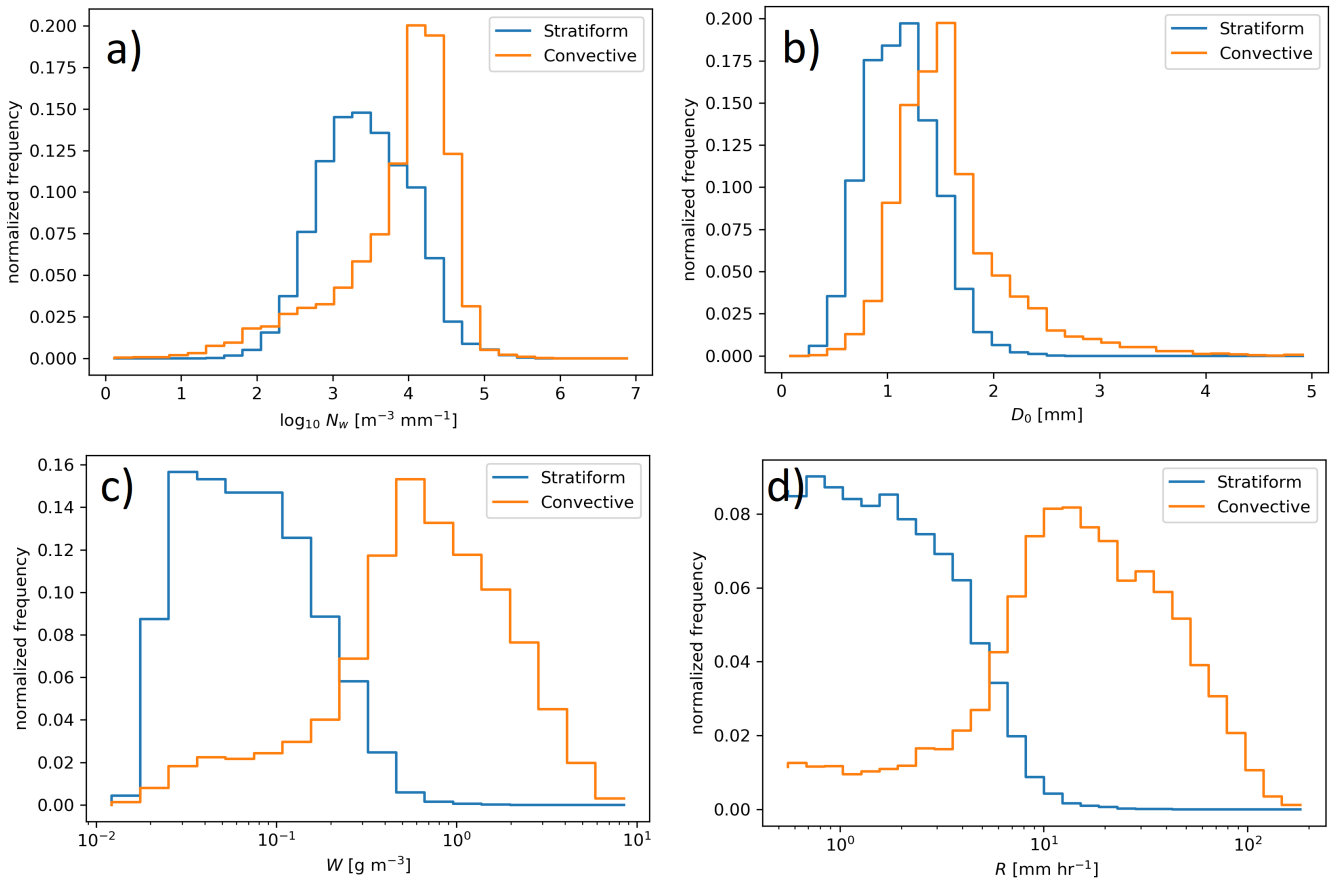

Figure 3. Normalized frequency histograms of **(a)** N_w, **(b)** D_0, **(c)** W, and **(d)** R separated by the BR09 stratiform-convective classification.

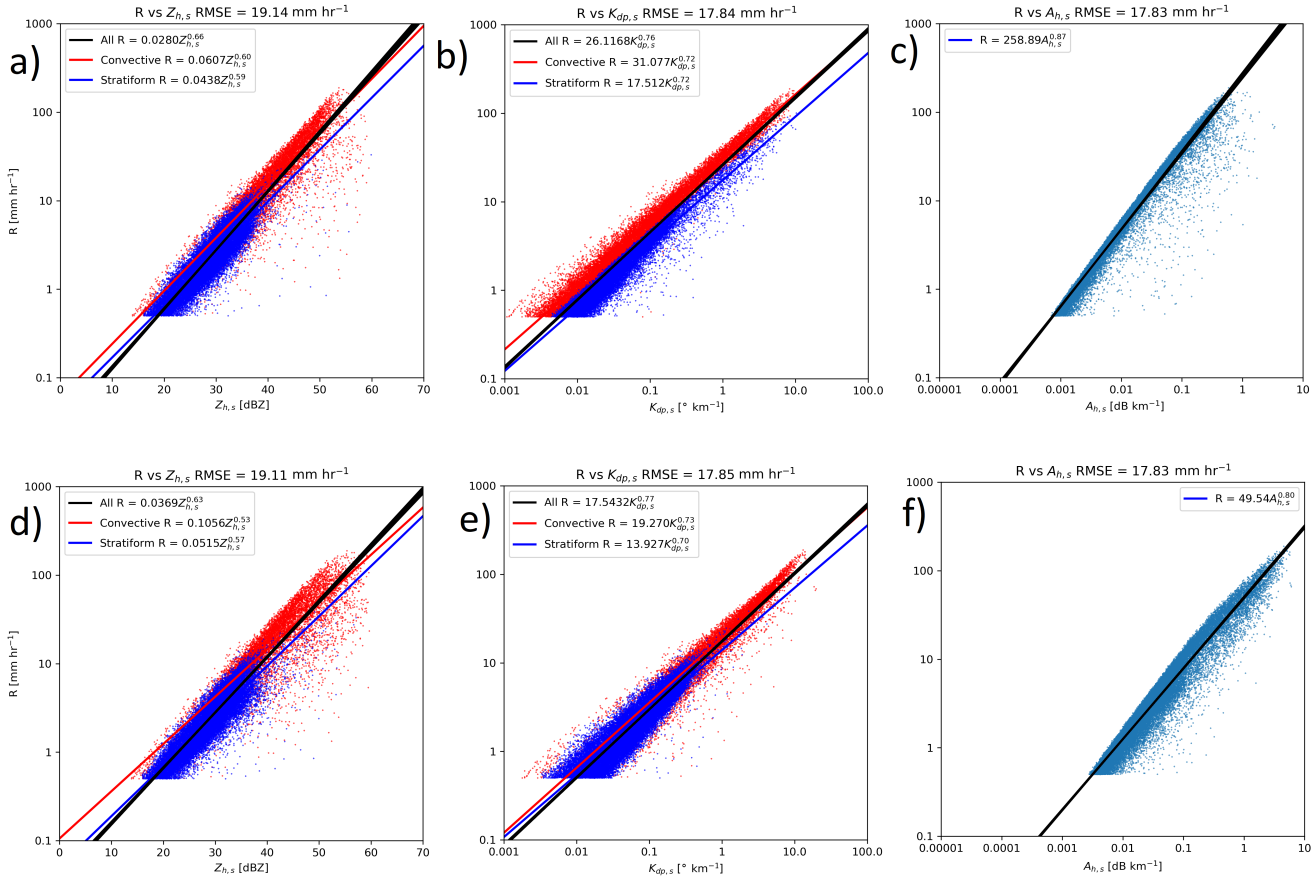

Figure 4. R from VDIS as a function of **(a)** Z_h, **(b)** A_h, **(c)** K_{dp}~~, for the simulated radar moments from VDIS at C-band. (d-f) as in (a-c) but for X-band. Each colored line represents a power law best fit of the variables. Each black line represents a fit produced by the bootstrap technique applied to the data in each panel.~~

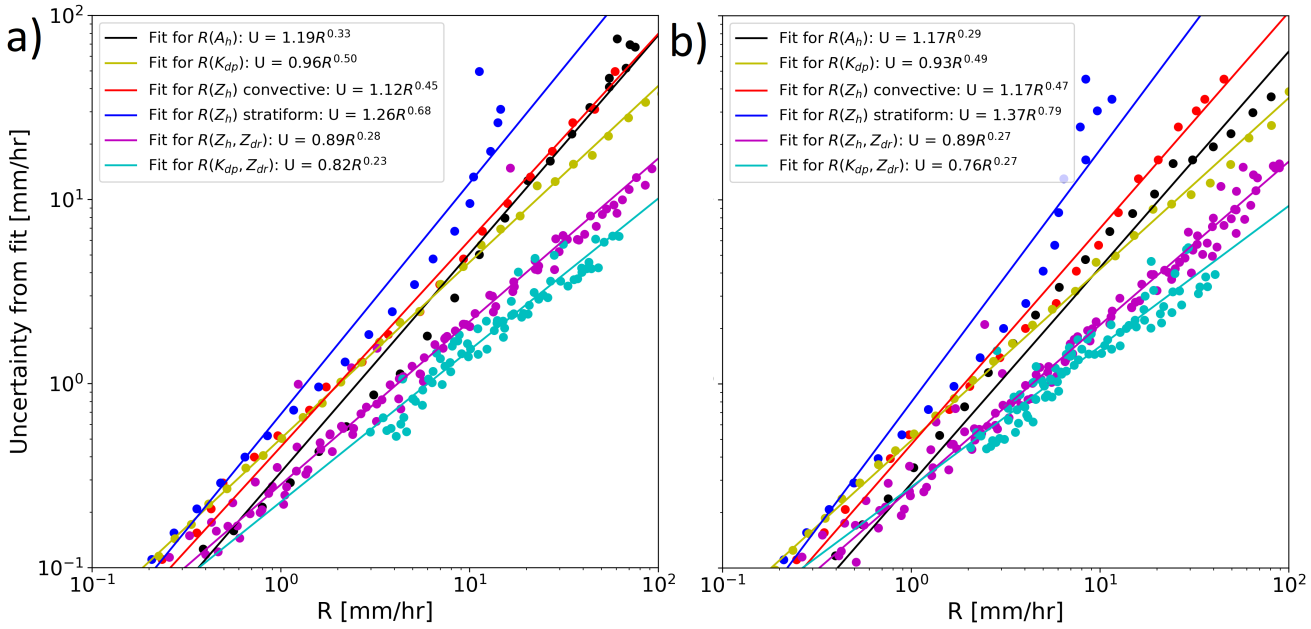

Figure 5. The spread in the p.d.f. of

, for the simulated radar moments from VDIS at C-band. **(d-f)** as in **(a-c)** but for X-band. Each colored line represents a power law best fit of the variables. Each black line represents a fit produced by the bootstrap technique applied to the data in each panel.

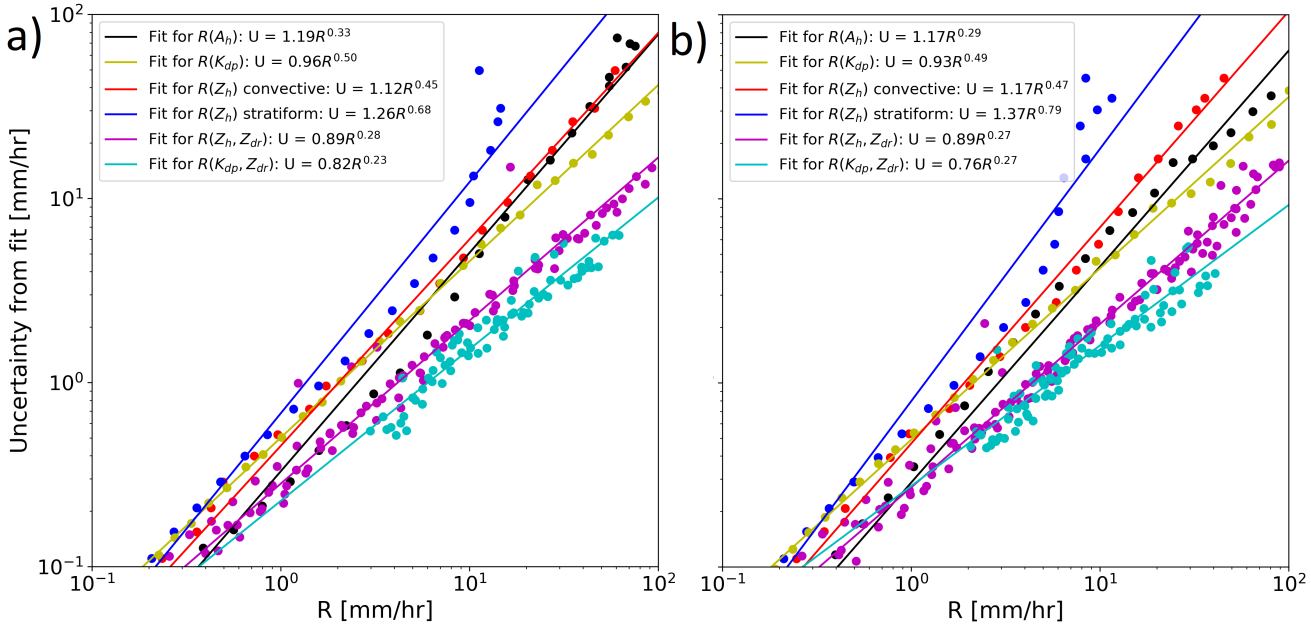

Figure 6. The parametric uncertainty of R estimated using the methodology of Kirstetter et al. (2015) as a function of mean R ~~for given ranges of radar moments at C-band **(a)**, and X-band **(b)**~~

.

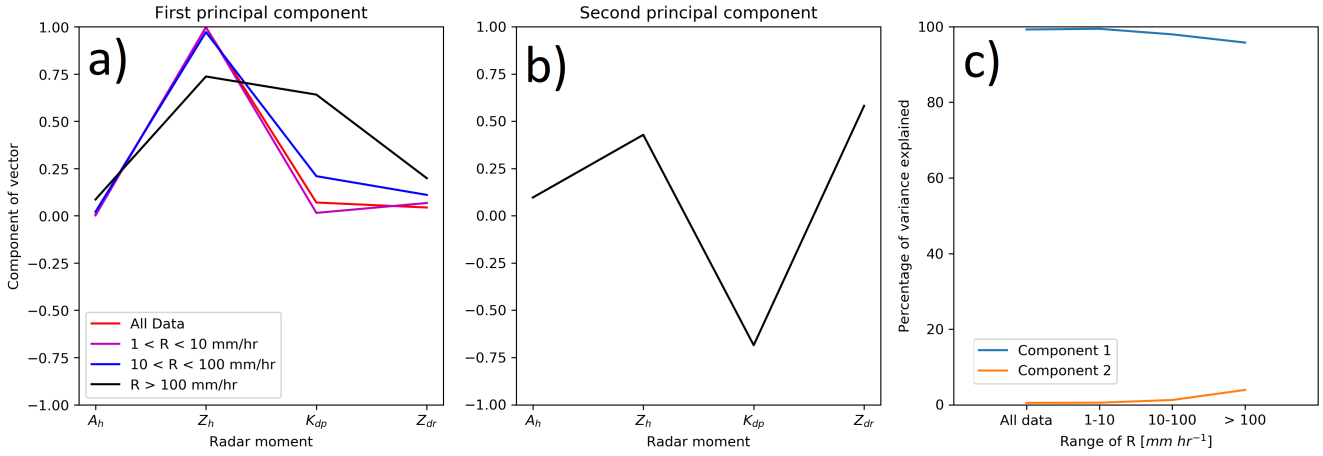

Figure 7. The first **(a)** and second **(b)** principal components of the simulated moments in (A_h, Z_h, K_{dp}, Z_{dr}) phase space for S-band. **(c)** shows the variance in R explained by each principal component for the C-band simulated moments.

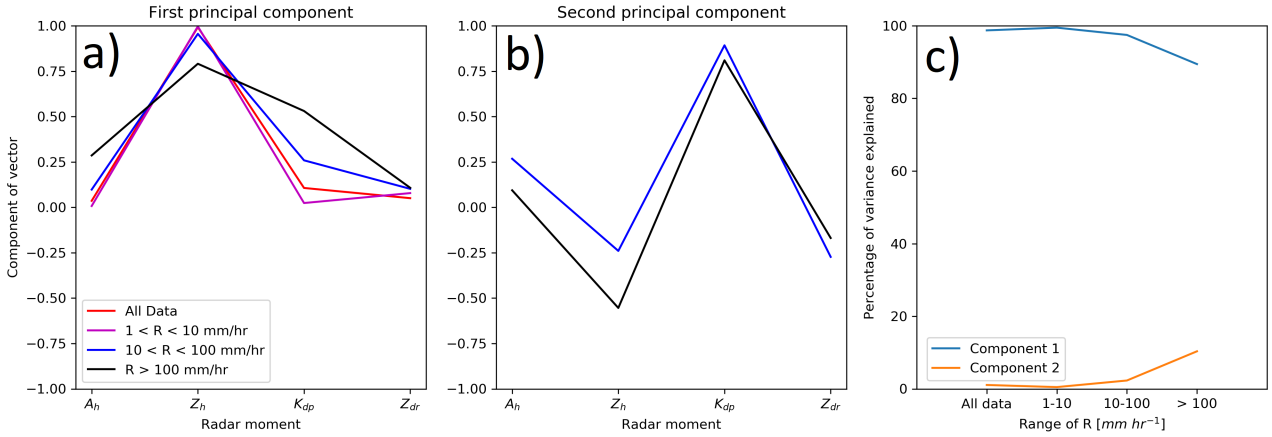

Figure 8. As Figure 10 but for X-band.

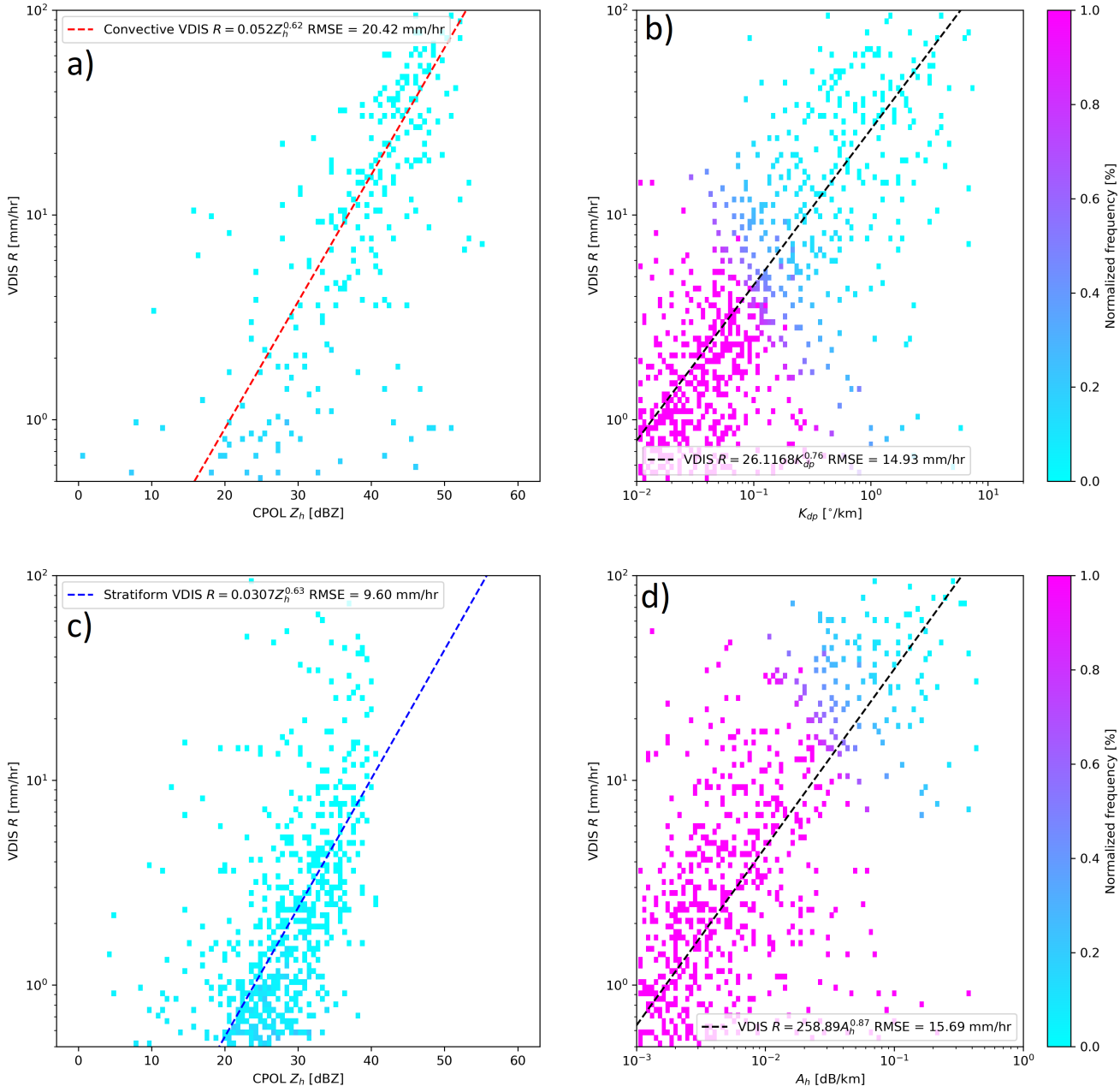

Figure 9. for given ranges of radar moments at C-band **(a)**, and X-band **(b)**

.

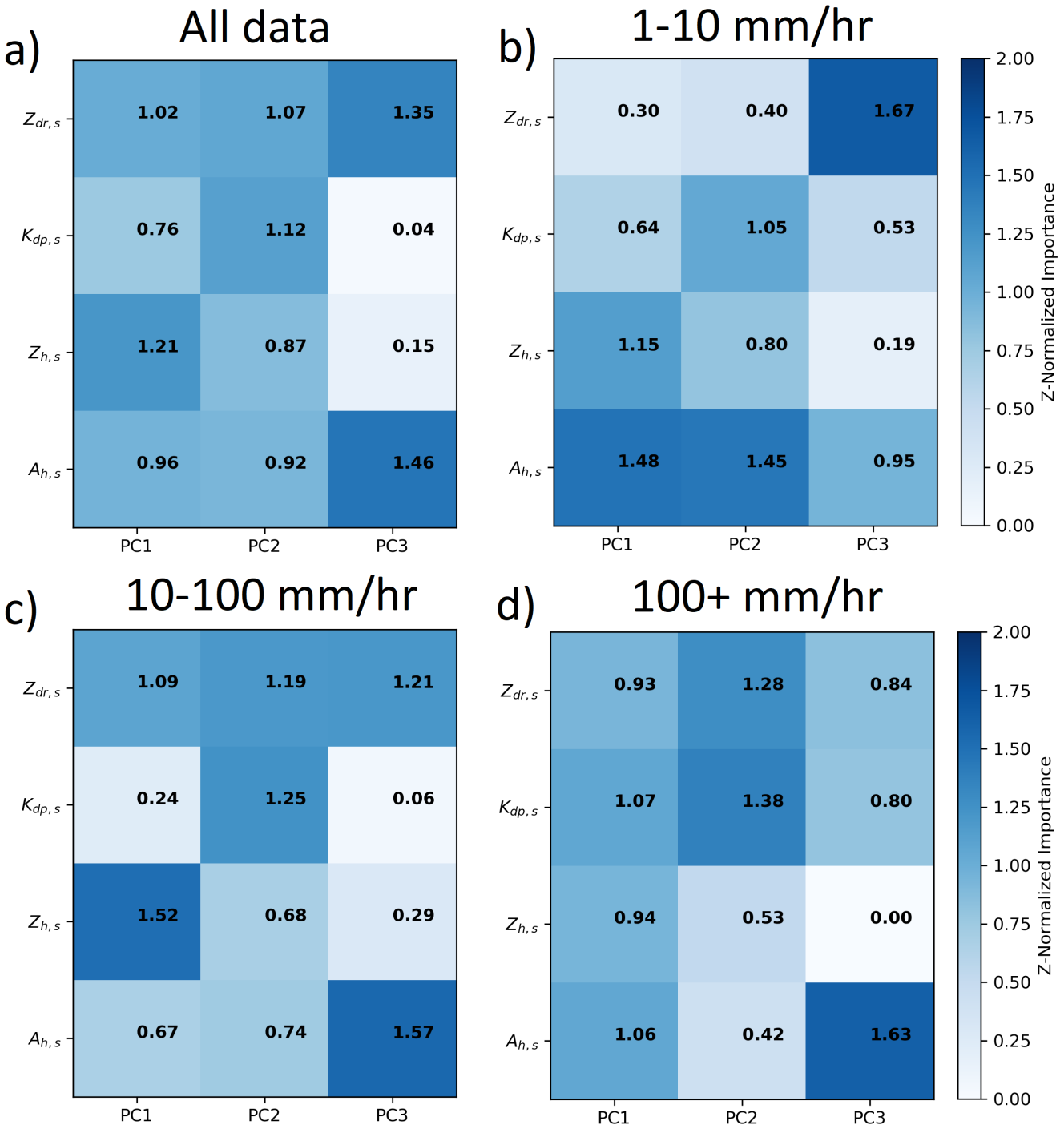

Figure 10. The variable importance matrix for the three principal components of $\underset{\sim}{\mathbf{X}}$ **(a)** *when all data is considered*, **(b)** *when* R *is 1 to 10* mm hr^{-1}, **(c)** 10 to 100 mm hr^{-1}, **(d)** more than 100 mm hr^{-1}

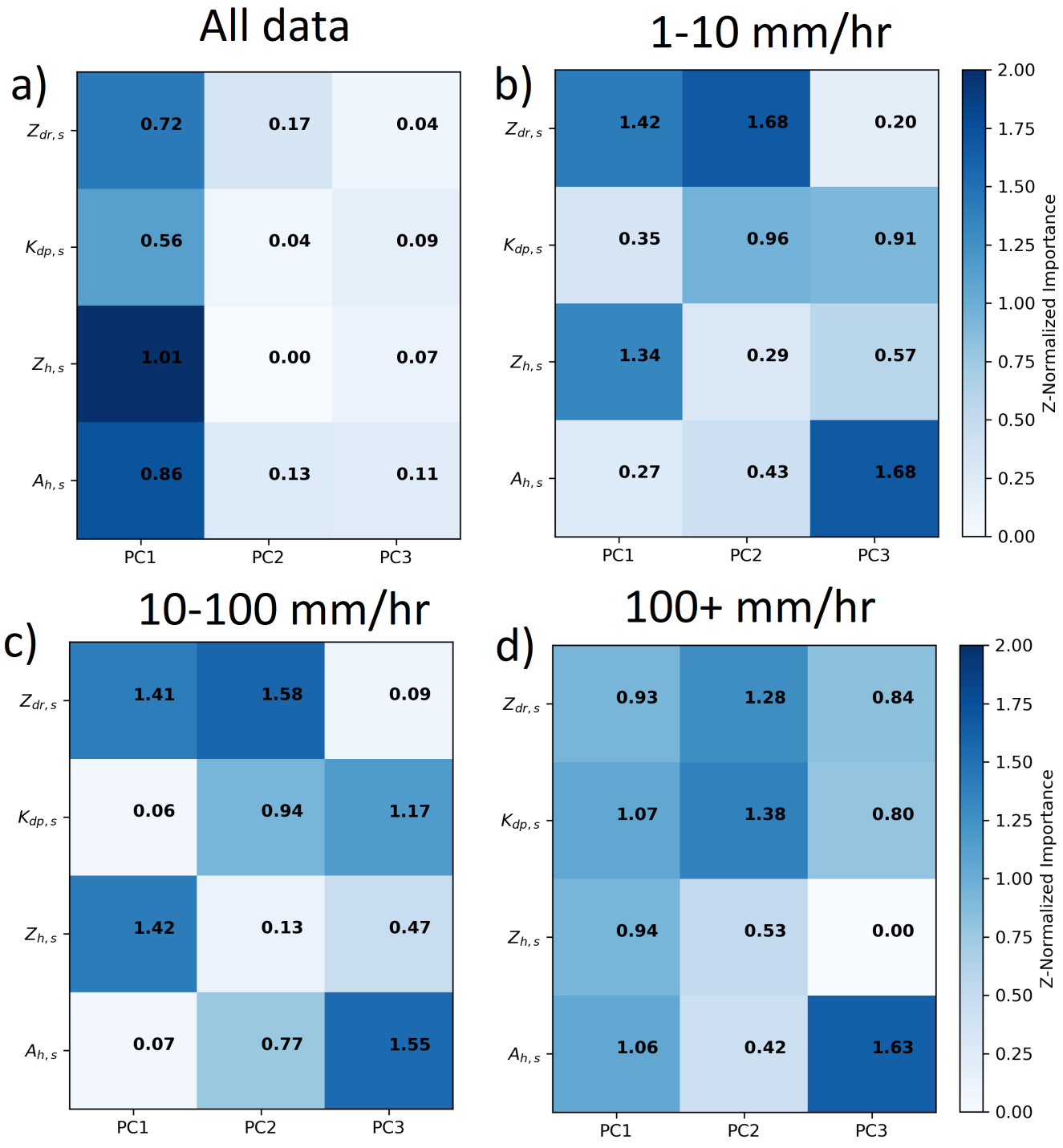

Figure 11. As Figure 10 but for X-band.

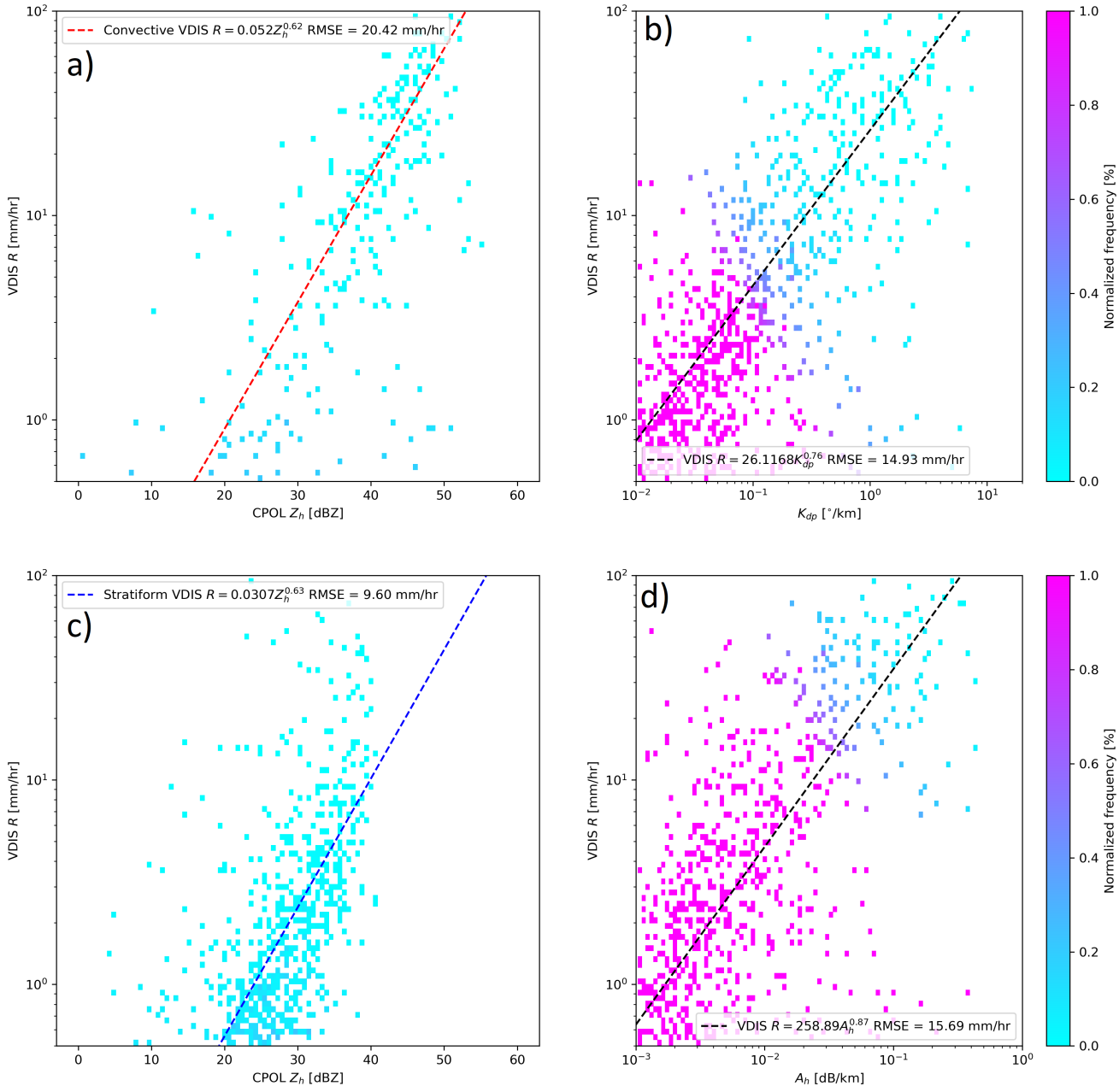

Figure 12. R from the VDIS as a function of **(a)** Z_h for convective DSDs, **(b)** K_{dp}, **(c)** Z_h for stratiform DSDs, and **(d)** A_h from CPOL. Solid lines are the R estimators in Figure 5.

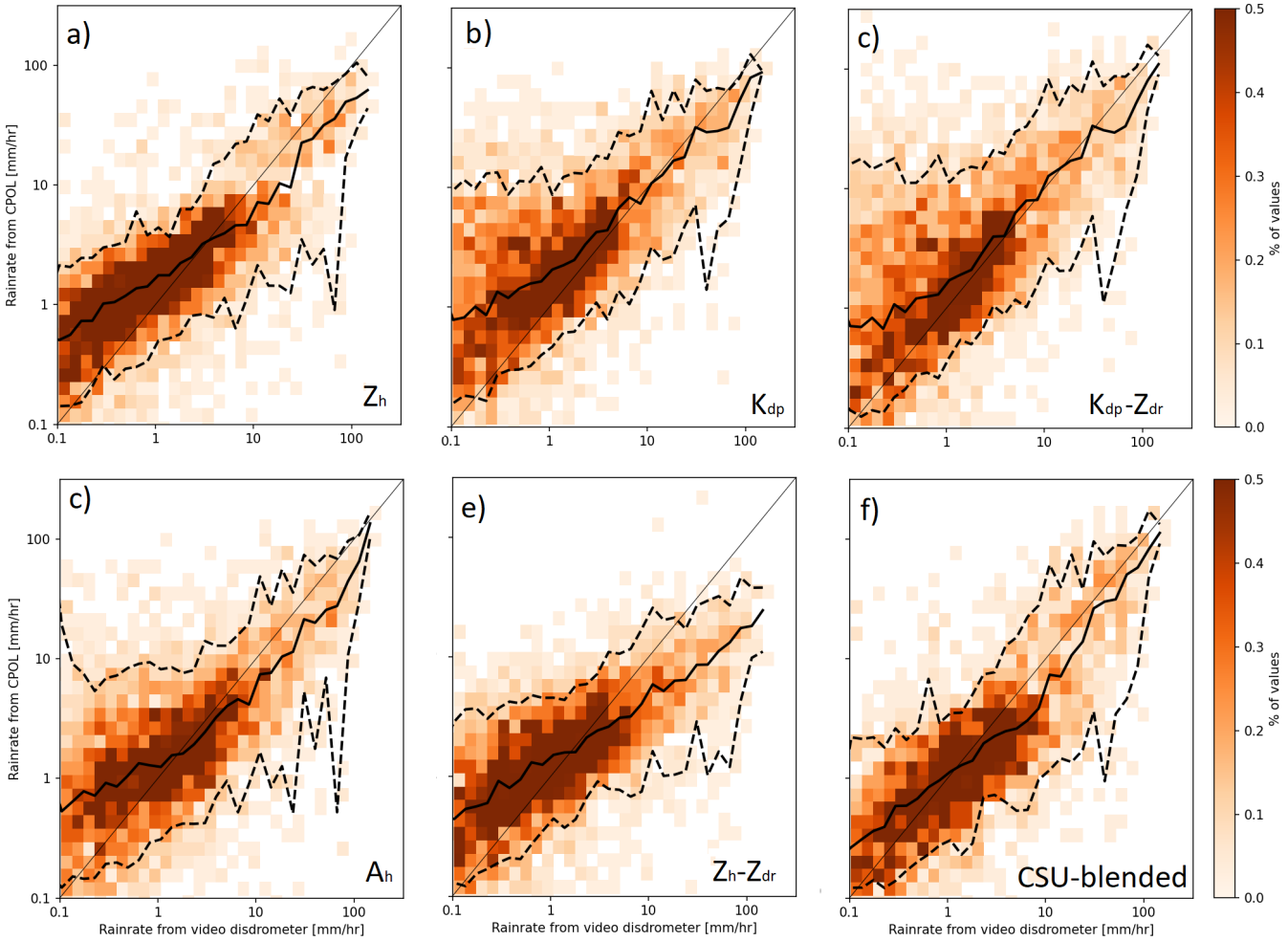

Figure 13. Normalized frequency distributions 10 minute averages of R estimated from the lowest gate from CPOL over VDIS using given estimators in Figure 5 as a function of 10 minute averages of R recorded by the VDIS. Estimators used to estimate R from CPOL are shown in each panel. Solid lines denote medians, dashed lines are the 5th and 95th percentiles of the estimated R from CPOL.